Thermal and Mechanical Analysis of High Power Microwave Windows

by

Philipp Michael Borchard

B.S.M.E., Massachusetts Institute Of Technology (1993)

Submitted to the Department of Mechanical Engineering
in partial fulfillment of the requirements for the degree of

Master of Science in Mechanical Engineering

at the

MASSACHUSETTS INSTITUTE OF TECHNOLOGY

June 1995

Author .....
Department of Mechanical Engineering
June 1995

Certified by .....
Doctor Richard J. Temkin
Senior Research Scientist, Physics Department
Thesis Supervisor

Certified by .....
Doctor Emanuel S. Bobrov
Lecturer, Mechanical Engineering Department
Thesis Reader

Accepted by .....
Professor Ain A. Sonin
Chairman, Departmental Committee

Thermal and Mechanical Analysis of High Power Microwave Windows

by

Philipp Michael Borchard

Submitted to the Department of Mechanical Engineering
on June 1995, in partial fulfillment of the
requirements for the degree of
Master of Science in Mechanical Engineering

Abstract

High Power microwave vacuum windows are an essential component in developing 1 MW/CW gyrotrons. The thesis focuses on thermal and mechanical analysis of three different microwave window designs. These include the present double disk window, a distributed window being developed by General Atomics and a single-disk diamond window design. The output microwave window is currently the limiting factor in obtaining high power ($\sim$ 1 MW) long pulse and cw operation. The present design has a maximum power handling capability of 450 kW.

The double disk window consists of two thin 12.7 cm sapphire disks which are face cooled by a fluorocarbon, which exhibits low microwave absorption. A thorough study of the present window has been made in order to learn more about the loss tangent, its temperature dependence and the film coefficient. 1D Analytical solutions for transient and steady state response of the double disk window have been developed as well as conducting 2 and 3D finite element simulations. The theoretical temperature calculations have been compared with temperature measurements of a sapphire double disk window that were conducted in conjunction with Varian Associates on a 500 kW gyrotron long pulse gyrotron and good agreement was found. 1 MW/CW power transmission is achievable by utilizing two double disk windows in a dual output configuration with a lowered peaking factor, or by employing the General Atomics Distributed or single disk diamond window.

Thesis Supervisor: Doctor Richard J. Temkin
Title: Senior Research Scientist, Physics Department

Thesis Reader: Doctor Emanuel S. Bobrov
Title: Lecturer, Mechanical Engineering Department

Acknowledgments

I would like to thank my thesis supervisor, Dr. Richard Temkin, for providing me with the opportunity to work on this project. I would also like to thank the scientists in the group, Drs. Kenneth Kreischer, Bruce Danly and Jean-Philippe Hogge for their support and help over the course of the project. I would also like to express my gratitude to Sam Chu, Marshall Loring and Kevin Felch at Varian Associates for their cooperation in the experimental temperature measurements of the S/N 4R1 gyrotron window. In addition like to thank Charles Moeller from General Atomics for his assistance in the analysis of the distributed Window. I would also like to thank all the students, especially Will Menninger whose programming skills provided invaluable assistance. Lastly, I thank Professor Emanuel Bobrov, my thesis reader.

Contents

List of Figures

List of Tables

Chapter 1

Introduction

1.1 Gyrotrons

The generation of high power millimeter wavelength radiation (traditional microwave range—see Fig. 1-1) is an important area of scientific research. Microwaves have many applications in modern society, ranging from military (radar, weapons systems) to industrial (communications, material processing, air traffic control radar) to domestic (microwave ovens, radar detectors). More specifically, in the high power regime, sources of microwave power are needed for applications such as heating hydrogen plasmas to several million degrees for the purpose of igniting a fusion reaction. Because of this demand, several high power microwave devices are currently under investigation. One of the most promising devices currently under investigation is the gyrotron. The gyrotron is an electron cyclotron resonance maser that operates throughout the microwave and millimeter region and emits coherent radiation at the electron cyclotron frequency or its harmonics. Gyrotron oscillators are capable of yielding much higher power levels at millimeter wave frequencies than conventional millimeter wave tubes. Their rf power producing capability lies at up to 5MW in the 100-300 GHz range. Although far infrared lasers operate in this region their efficiencies in this regime are less than 0.1%.

In the gyrotron, electrons are produced by a magnetron injection gun (MIG) and

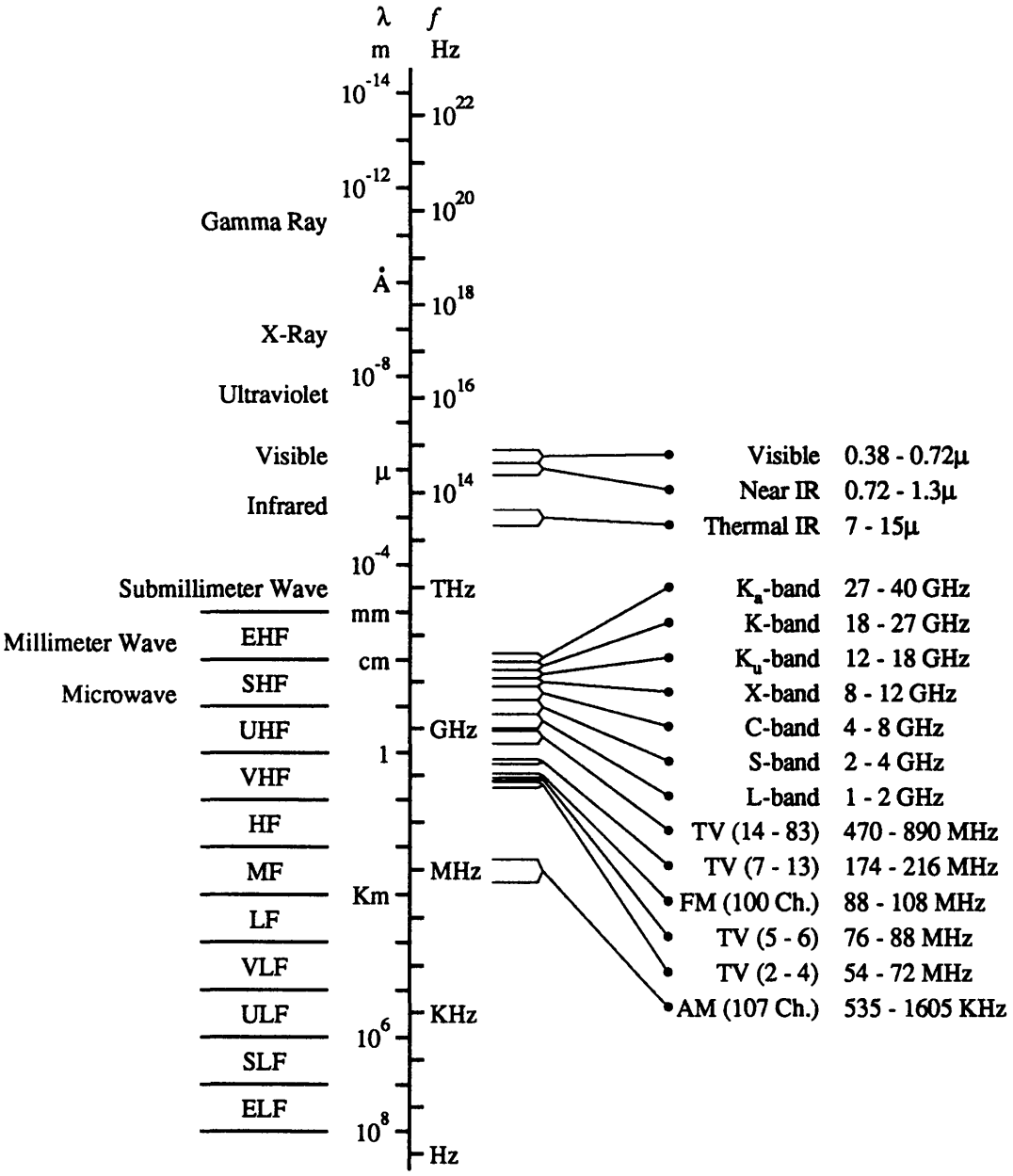

Figure 1-1: The Electromagnetic Wave Spectrum [15].

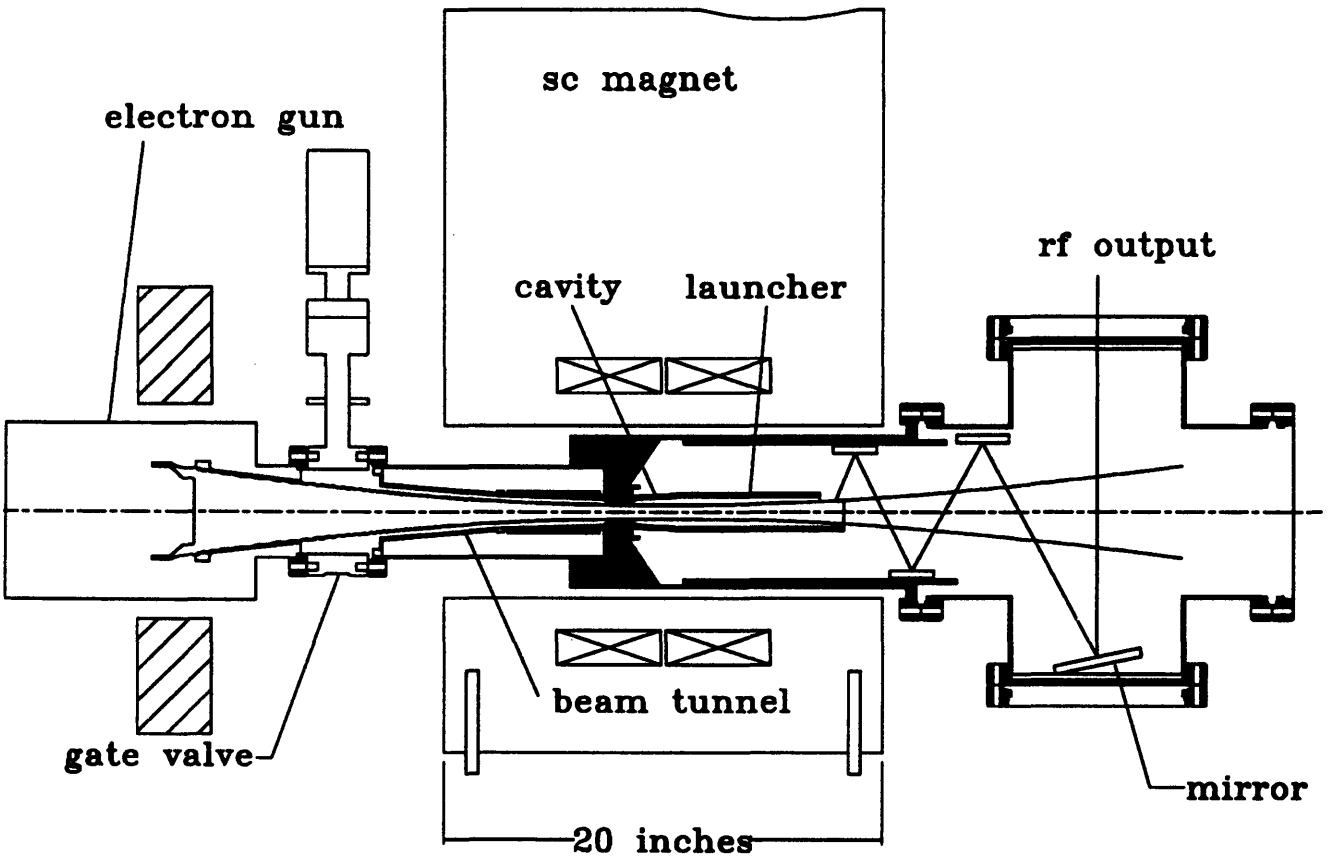

Figure 1-2: Schematic of the ITER Gyrotron

accelerated by a potential difference across the anodes. The produced electrons follow the magnetic field lines into the cavity region. The high rf energy produced within the gyrotron is a result of an energy exchange, within the interaction cavity, between electrons orbiting in a magnetic field and EM waves with transverse component of electric field at the cyclotron frequency. The electrons continue along the magnetic field lines until they are deposited on the walls of the collector. The RF field travels down the collector and is transmitted through the window. Operating parameters for a gyrotron are typically 80 kV at the gun and 40 A collector current [16]. A schematic of the gyrotron is shown in figure 1-2.

Current gyrotron oscillator tubes used for electron cyclotron heating (ECH) heating of plasmas are capable of delivering about 200 kW in pulsed operation ($\leq$ 3 sec). Future experiments, such as ITER require 20-50 MW ECH power at 170 GHz in continuous operation (CW) to be supplied to the plasma. In order to make gyrotrons a

feasible source as well as to reduce the total number of units required, each gyrotron has to be capable of 1MW/CW operation.

For the vacuum seal of the gyrotron, as well as that of the plasma torus heavy-duty dielectric windows are needed. These windows need to be cooled to dissipate the RF energy absorbed in the dielectric. The aim of this thesis is to give an overview of the different kinds of windows used today and those currently under development. Particular focus is directed to face-cooled double disk and edge-cooled single disk windows. The output microwave window is currently the limiting factor in obtaining ($\sim$ 1 MW) long pulse and CW operation. There is a need for a microwave vacuum window for ITER capable of transmitting 1 MW at 170 GHz.

1.2 Thesis Organization

Chapters 2–5 of this thesis are organized as follows:

Chapter 2 presents three gyrotron window designs and examines the thermal and mechanical analysis of these window types.

Chapter 3 presents the results of the experimental temperature measurements of a double disk sapphire window.

Chapter 4 discusses the thermal and structural finite element analyses of the various window designs and compares these results to the results presented in Chapter 3.

Finally in Chapter 5 conclusions are drawn.

Chapter 2

Theory

2.1 Introduction

A microwave window, for gyrotron applications, is needed capable of transmitting significant amounts of microwave energy without exhibiting thermal runaway. The window must be able to withstand the thermally induced stresses caused by the temperature rise of the window as well as the mechanical stresses caused by atmospheric and coolant pressure.

2.2 Gyrotron Microwave Windows

The present gyrotron window is a double disk sapphire window as shown in Figure 2-1. The sapphire window consists of two thin disks 12.7 cm in diameter with a 0.698 mm gap inbetween them. The sapphire disks are faced cooled by a fluorocarbon which is pumped through the window gap. A new design is currently under development by General Atomics. This distributed window consists of parallel niobium fins with a spacing of approximately one wavelength. Sapphire pieces are brazed inbetween the fins through which the microwaves pass. The window is cooled by passing water through cooling channels which are integrated into the fins. A schematic of the window is shown in Figure 2-2. A third design is a diamond window with water edge cooling. Diamond grown by chemical vapor deposition (CVD) is becoming a

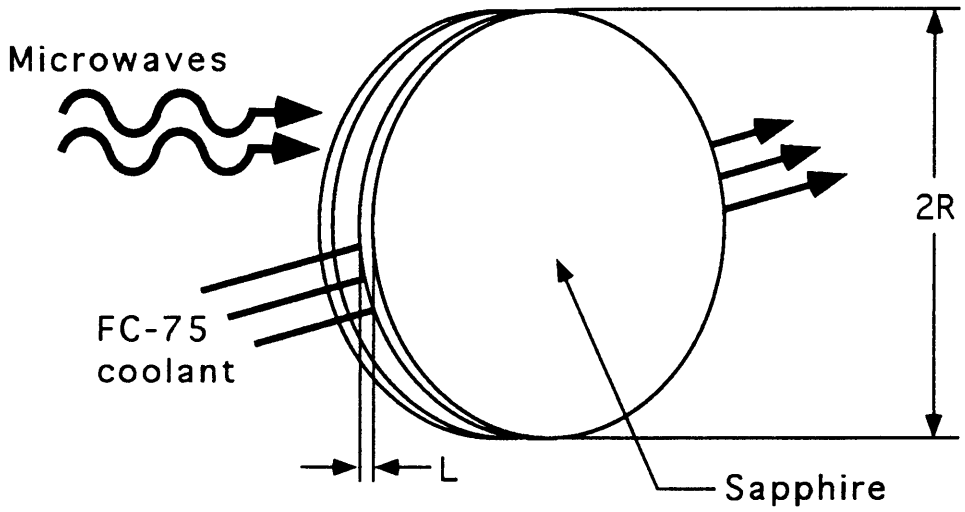

Figure 2-1: Schematic of Double Disk Sapphire Window

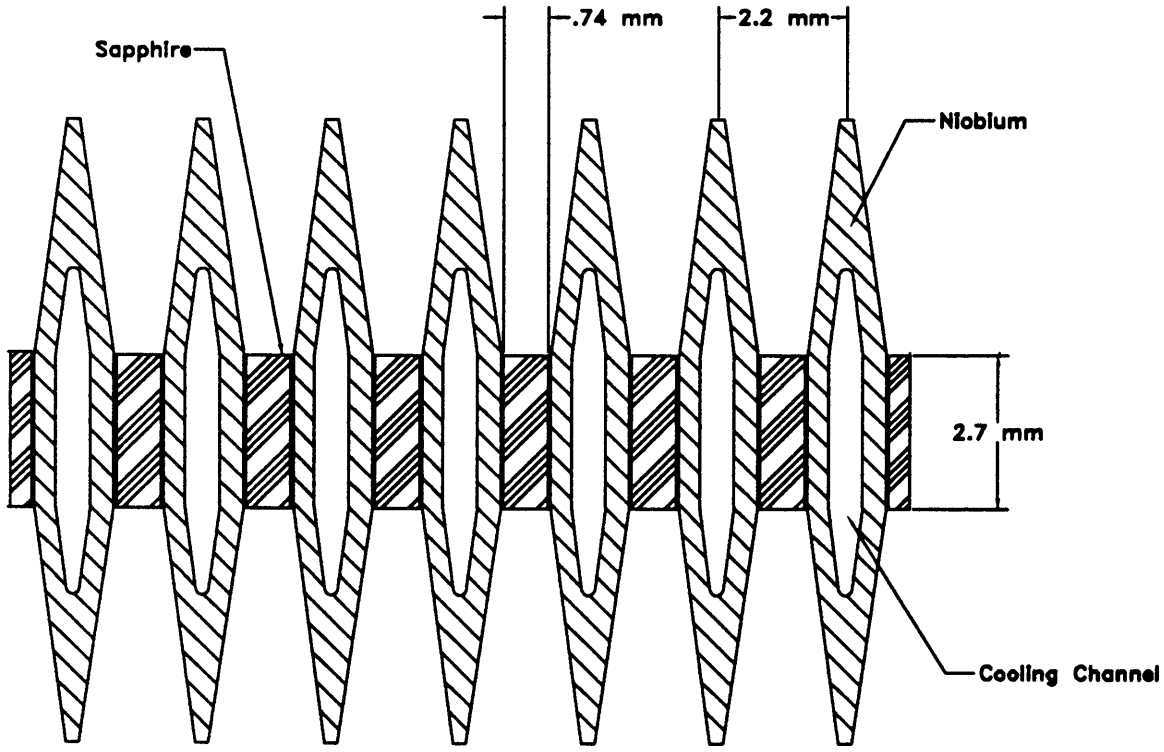

Figure 2-2: Schematic of General Atomics Distributed Window

	Material	
Material Properties	Sapphire	Synthetic Diamond
Density $\frac{g}{cm^3}$	3.98	8.5
Youngs Modulus GPa	340	1050
Tensile Strength MPa	350	1000
Compressive Strength MPa		~1000
Thermal Conductivity $\frac{W}{mK}$ 300K	38	1300
Thermal Diffusivity $\frac{cm^2}{s}$	0.123	2.97
Thermal Expansion $10^{-6}K^{-1}$	8	0.8
Heat Capacity $\frac{J}{gK}$	0.764	0.516
Poisson's Ratio	.29	~0.2
Permittivity $\epsilon_r^{'}$	9.7	5.7
Loss Tangent tanδ 10^{-4} 110GHz	1.5	0.87

Table 2.1: Material Properties [5].

viable window material, as the ability to manufacture large high quality diamond disks with good microwave properties is being developed. A window of this kind would incorporate a diamond disk between 5 and 7.5 cm in diameter with a thickness of approximately 1 mm.

One of the difficulties in analyzing the thermal performance of these gyrotron windows is the relative scarcity of data for the loss tangent, tanδ, of the sapphire and the diamond at frequencies of 110 to 170 GHz. Measurements of the loss tangent of diamond and sapphire have been made [9, 20, 4]. However, the loss tangent is dependent on properties such as surface finish, material grade and the thickness tolerance. Actual temperature measurements of the gyrotron window have been few so far [14]. In chapter 3 temperature measurements of a double disk window in operation are made. To conduct these measurements a long wave infrared camera was utilized. The measurements are made more difficult by the fact that sapphire only has strong thermal emission in the long wave infrared spectrum (8 to 12 μm) and by the presence of several hundred kilowatts of microwave power passing through the window. The material properties utilized in the thermal and mechanical analysis are shown in Table 2.1.

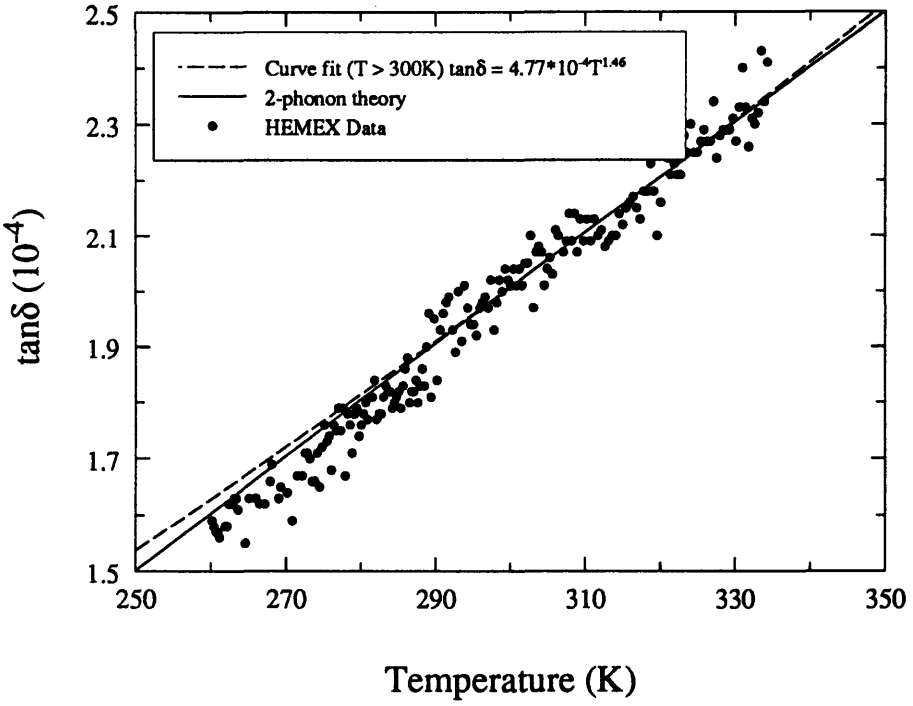

Figure 2-3: Loss tangent data for Sapphire at 145 GHz [9]

Heidinger's data [9] for the loss tangent of sapphire at 145 GHz is shown in Figure 2-3. At 145 GHz the loss tangent is $2.0 \cdot 10^{-4}$ at 300 K. A curve fit for the sapphire loss tangent data above 300 K gave a temperature dependence of about $T^{1.46}$. With a frequency to the first power scaling for the loss tangent this gives an effective loss tangent of $1.5 \cdot 10^{-4}$ at 110 GHz.

The loss tangent data for various diamond grades at 145 GHz is shown in Figure 2-4. The loss tangent is inversely proportional to the frequency squared [10]. For the diamond loss tangent of $8.7 \cdot 10^{-5}$ with a temperature dependence of T^2 was utilized.

2.3 RF Power losses in the window

The power profile in the output window can take a variety of shapes. The most desirable profile is Gaussian distribution, which simplifies coupling the beam into a corrugated waveguide for transport to the plasma, a Gaussian is also needed for current control and heating of the plasma. For a Gaussian distribution the power flux

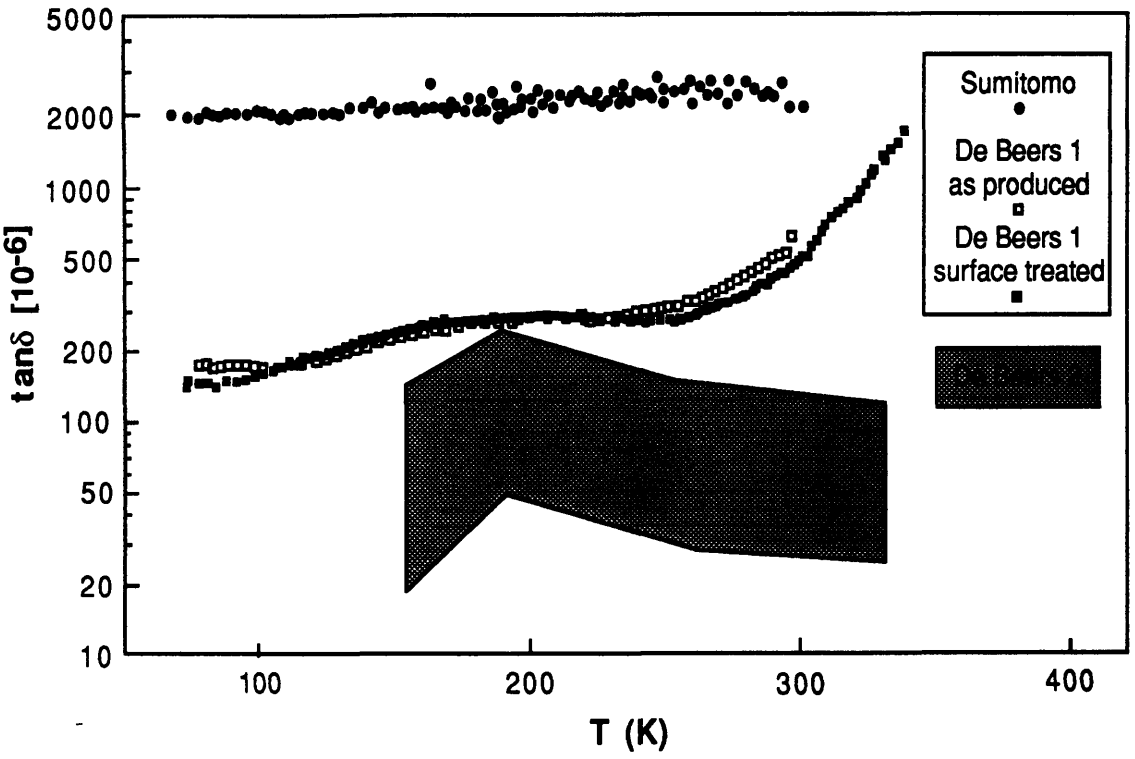

Figure 2-4: Loss tangent data for various CVD Diamond Specimen [10]

impinging on the window is given by [21]

$$I(r) = \frac{P_{in}}{\pi R^2} \exp\left(-\frac{r^2}{a^2}\right) \tag{2.1}$$

where R is the window radius and a is the beam spot size. The disadvantage of the Gaussian profile is the high peaking factor E_{mp}. The peaking factor is defined by equation 2.2

$$E_{mp} = \frac{\text{Peak Intensity}}{\text{Average Intensity}} \tag{2.2}$$

For a Gaussian distribution the peaking factor is typically between 4.1 and 5.6 for a circular window. High peaking factors cause hot spots on the window which limit the maximum power handling capability of the window due to thermal runaway and the fact that the maximum temperature of the window at any location is limited. Lowering the peaking factor gives a proportional increase in the power handling capability as given by equation 2.3.

$$P_{max}\alpha\frac{1}{\text{Peak Intensity}} \tag{2.3}$$

The aim has therefore been to decrease the peaking factor by designing mode converters which produce a ring distribution as given by equation 2.4 at the window. The benefits are twofold, a significant reduction of the peaking factor is possible to values around two, as well as reducing the intensity at the center of the window. The double disk window in particular would benefit, as the film coefficient at center is reduced due to the deflection of the sapphire disks due to the coolant pressure.

$$I(r) = \frac{P_{in}}{\pi R^2}(ar^3 + br^2 + cr + d) \tag{2.4}$$

The RF losses in the window are given by the equation 2.5

$$\alpha_o = \frac{2\pi f}{c}\sqrt{\epsilon'}tan\delta S \tag{2.5}$$

where α_o is the absorption loss m^{-1}, f is the gyrotron output frequency, c is the speed of light and ϵ' is the refractive index [24]. S is the enhancement factor in the absorption due to the fact that the windows are acting as Fabry-Perot. S is close to unity when the window is made antiresonant (which requires a tolerance on the window thickness of 0.004 mm for the 110 GHz case). For the case of resonant power transmission, which will be considered here, S is given by equation 2.6.

$$S = \frac{(1+\epsilon')}{2\sqrt{\epsilon'}} \tag{2.6}$$

The enhancement factor is about 1.7 for a single sapphire disk in a double disk window [21].

2.4 Thermal and Mechanical Analysis

The different windows can be divided into cylindrical and rectangular types. For cylindrical windows such as the sapphire double disk and diamond single disk window

a cylindrical coordinate system was employed. The temperature distribution within a flat cylindrical window is a function of spatial coordinates (r, θ, z). The exact form of the distribution can be determined by solving the general heat conduction equation 2.7 in cylindrical coordinates.

$$\frac{\partial^2 T}{\partial r^2} + \frac{1}{r}\frac{\partial T}{\partial r} + \frac{1}{r^2}\frac{\partial^2 T}{\partial \theta^2} + \frac{\partial^2 T}{\partial z^2} + \frac{q(r)}{k} = \frac{1}{\alpha}\frac{\partial T}{\partial t} \tag{2.7}$$

where T is the temperature, k the thermal conductivity, α is the thermal diffusivity and q the volumetric heat generation which is given by equation 2.8.

$$q(r) = \alpha_o I(r) \tag{2.8}$$

During the operation of the gyrotron window high electric fields are established within the window. As current window materials exhibit finite dielectic losses, energy is absorbed and significant quantities of heat can be generated within the window. The heat generation in the window due to RF power deposition and the surface cooling determine the radial and axial temperature profile. Once the temperature distribution has been found the radial and tangential stresses can be determined. Since the temperature distribution depends on a complex fashion on both r and z finite element solutions are generally employed [7, 6].

2.5 Double Disk Window

Thermal and stress analysis of the double disk window was carried out for a Gaussian distribution, a ring distribution and the actual distribution as recorded with an infrared camera. The objective of the double disk evaluation was to determine the relevant parameters for the thermal and mechanical behaviour of the window. These parameters were then utilized to determine the optimal compromise between window size, intensity profile and cooling condition which permit the highest power transmission [19].

The thickness of the sapphire disks is dictated by the need to minimize the re-

flection and absorption of the microwave beam. This means that the thickness is a multiple of the half-wavelength in the window material. The thickness is given by equation 2.9

$$L = n\frac{\lambda}{2}\frac{1}{\sqrt{\epsilon'}} \qquad n = 1, 2, 3, ... \tag{2.9}$$

where λ is the free space wavelength of the of the microwave beam. To ensure that the temperature and temperature gradients within the sapphire window are not excessive, face cooling is required. The cooling medium is typically a commercial fluorocarbon liquid (FC-75) which is chosen based on its low viscosity and low energy absorption in the microwave frequency range [1]. For a face cooled window design it is essential to reduce the thickness of the window to a minimum, while maintaining adequate strength to withstand the coolant pressure of the fluorocarbon coolant. The temperature limitation on the window is imposed by the boiling point of the coolant. When the surface temperature of the sapphire at the coolant interface begins to exceed the saturation temperature of the FC-75, boiling occurs. In the nucleate boiling regime the surface heat flux dramatically increases, however after the critical heat flux is reached the surface heat flux drops dramatically as the boiling transitions into the film regime. To avoid thermal runaway and subsequent window breakage, the maximum allowable temperature is limited to the saturation temperature of the FC-75 coolant which is ~395 K under nominal flow conditions (a coolant flowrate Q_{FC} of 0.85 l/s).

The window boundaries consist of two parallel faces one of which is isolated and the heat flow across the other face is given by equation 2.10.

$$q = h(T_s - T_b) \tag{2.10}$$

where h is the film coefficient, T_s the surface temperature of the sapphire and T_b the bulk temperature of the coolant. The edges of the sapphire disk are assumed to be isolated. A curve fit of the thermal conductivity data of sapphire [23] was used to obtain the temperature dependence of the sapphire thermal conductivity as given by

equation 2.11.

$$k = 10.5\exp\left(\frac{430K}{T}\right)\frac{\text{watt}}{\text{mK}} \tag{2.11}$$

The film coefficient of the structure was determined from the analytical turbulent flow theory. The dimensionless Reynolds number, which represents the ratio of the inertial to the viscous forces of the flow is given by equation 2.12

$$Re = \frac{D_h \rho v}{\mu} \tag{2.12}$$

where ρ is the density, μ is the viscosity of the coolant and v is the mean coolant velocity. D_h is the hydraulic diameter of the cooling passage and is given by $D_h = \frac{4A_c}{P}$, where A_c is the cross-sectional area and P the perimeter of the cooling channel. The dimensionless Prandtl number is given by equation 2.13 The Prandtl number provides a measure of the relative effectiveness of momentum and energy transport by diffusion in the thermal and velocity boundary layers.

$$Pr = \frac{C\mu}{k_c} \tag{2.13}$$

where C is the specific heat capacity and k_c is the thermal conductivity of the coolant. From the dimensionless Reynolds and Prandtl number we can obtain the dimensionless Nusselt number for turbulent flow conditions ($Re > 10,000$) from equation 2.14 [8].

$$Nu = \frac{\frac{f}{8}(Re - 1000)Pr}{1.07 + 12.7\left(\frac{f}{8}\right)^{0.5}(Pr^{0.67} - 1)} \tag{2.14}$$

where f is the friction factor given by equation 2.15 for smooth surfaces. The friction factor can also be obtained for a wide range of Reynolds numbers from the Moody diagram [18].

$$f = 0.79\ln(Re - 1.64)^{-2} \tag{2.15}$$

From the Nusselt number we can then obtain the film coefficient by equation 2.16

$$h = \frac{k_c Nu}{D_h} \tag{2.16}$$

For a flow rate of 0.95 l/s a theoretical film coefficient of 7.5 kW/m^{2}K was obtained.

A nominal window radius of 12.7 cm with a 10.16 cm effective waveguide diameter was considered. The window was initially analyzed using analytical and numerical 1D solutions, as well as 2 and 3D finite element analysis. While the 1D axial solutions tend to overestimate the temperature rise, due to the neglect of the radial and azimuthal heat conduction, they offer a fast approach for evaluating the relevant parameters in the window configuration.

2.5.1 Steady State

For the double disk window the analytical 1D axial solution is reducing the 3D heat equation 2.7 to a 1D axial heat equation 2.17. The boundary conditions for the 1D heat equation are given by equations 2.18.

$$\frac{d^2T}{dz^2} + \frac{q}{k} = 0 \tag{2.17}$$

$$\begin{aligned} -k\frac{dT}{dz}\bigg|_{z=L} &= h(T_s - T_b) \\ \frac{dT}{dz}\bigg|_{z=0} &= 0 \end{aligned} \tag{2.18}$$

$$\Delta T_s(z) = \frac{\alpha_o I}{k(T)}(L^2 - z^2) \tag{2.19}$$

ΔT_s is the temperature drop across the sapphire which is obtained by solving the 1D heat equation.

$$T_s = \frac{\alpha_o I L}{h} \tag{2.20}$$

T_s is the surface temperature of the cooled face of the sapphire disk. It is obtained

by evaluating the boundary condition given by equation 2.18. The total steady state temperature is then given by equation 2.21 by combining the terms from equations 2.19 and 2.20.

$$T_{max}(z) = \frac{\alpha_o I}{k(T)}(L^2 - z^2) + \frac{\alpha_o I L}{h} \tag{2.21}$$

2 and 3D solutions were obtained by using the ANSYS finite element software.

2.5.2 Transient Analysis

For the transient response an analytical 1D expression, a 1 and 2D numerical simulation and a 2 and 3D finite element analysis were utilized.

The one-dimensional analytical transient solution can be found by non-dimensionalizing the variables. The following dimensionless variables were defined.

$$z^* = \frac{z}{L} \tag{2.22}$$

$$\theta^* = \frac{\theta}{\theta_f} = \frac{T - T_b}{T_f - T_b} \tag{2.23}$$

where T_b is the coolant temperature and T_f is the steady state temperature of the sapphire.

$$t^* = \frac{\alpha t}{L^2} = \mathrm{Fo} \tag{2.24}$$

$$\mathrm{Bi} = \frac{hL}{k} \tag{2.25}$$

where Fo and Bi are the dimensionless Fourier and Biot numbers. Substituting these dimensionless variables into the heat equation 2.7, equation 2.26 is obtained.

$$\frac{\partial^2 \theta^*}{\partial z^{*2}} = \frac{\partial \theta^*}{\partial \mathrm{Fo}} \tag{2.26}$$

The boundary condition (equations 2.18) become

$$\left.\frac{\partial\theta^*}{\partial z^*}\right|_{z^*=0} = 0$$
$$\left.\frac{\partial\theta^*}{\partial z^*}\right|_{z^*=1} = -\mathrm{Bi}\theta^*(1,t^*) \tag{2.27}$$

To solve equation 2.26 it is necessary to specify a final condition in addition to the two boundary conditions. The final condition is the final steady-state temperature profile as given by equation 2.21.

$$\theta_f(z^*,\infty) = T_{max}(0) \tag{2.28}$$

The transient axial analytical solution of equation 2.7 is then given by equation 2.29.

$$\theta^* = \sum_{n=1}^{\infty} C_n \exp\left(-\zeta_n^2 \mathrm{Fo}\right)\cos\left(\zeta_n z^*\right) \tag{2.29}$$

where ζ_n are the positive roots of the transcendental equation $\zeta_n \tan(\zeta_n) = \mathrm{Bi}$ and C_n is given by equation 2.30.

$$C_n = \frac{4\sin(\zeta_n)}{2\zeta_n + \sin(2\zeta_n)} \tag{2.30}$$

The transient temperature rise in terms of normalized location and time is then given by equation 2.31,

$$T(z^*,t^*) = (1-\theta^*)T_{max}(0) \tag{2.31}$$

The transient analytical model is only valid for temperature independent values of the loss tangent, film coefficient and thermal conductivity. In order to accommodate the temperature dependence of these variables a numerical simulation code was written. The code is a 1 or 2D finite difference code. For the 1D case the one-dimensional heat equation was solved, by dividing the window thickness axially into multiple sections. The energy balance method was applied to a control volume around each node.

The inputs consists of the microwave power absorbed by each section and heat flow into it from adjacent sections. The output consists of the thermal conduction to adjacent sections and the temperature rise of the section. From the energy balance we get equation 2.32.

$$T_m^{p+1} = \mathrm{Fo}[T_{m-1}^p + T_{m+1}^p + \frac{q(\Delta z)^2}{k}] + [1 - 2\mathrm{Fo}]T_m^p \tag{2.32}$$

For the section at the coolant interface the equation 2.33 is obtained.

$$T_m^{p+1} = 2\mathrm{Fo}[T_{m-1}^p + \mathrm{Bi}T_{coolant} + \frac{q(\Delta z)^2}{k}] + [1 - 2\mathrm{Fo} - 2\mathrm{BiFo}]T_m^p \tag{2.33}$$

where m is the section index and p is the time step. Fo and Bi are the dimensionless Fourier and Biot numbers as defined above. The timestep for the numerical simulation was obtained from the stability condition imposed by equation 2.33. The coefficient of T_m^p must be greater than or equal to zero, therefore

$$\begin{aligned} 1 - 2\mathrm{Fo} - 2\mathrm{BiFo} &\leq 0 \\ \textit{or} & \\ \mathrm{Fo}(1 + \mathrm{Bi}) &\leq \frac{1}{2} \end{aligned} \tag{2.34}$$

The Biot number was determined at T_o and an appropriate Fourier number was chosen as to satisfy equation 2.34. From the Fourier number we can determine the timestep per iteration. For the numerical simulation a number of factors and their effect on the transient response were studied. The temperature dependence of the thermal conductivity, loss tangent and film coefficient were analyzed and incorporated into the simulation.

2.5.3 Mechanical Analysis

The temperature distribution obtained in the 2 and 3D thermal analysis, was incorporated into a finite element analysis to determine the thermal and mechanical loading

of the window. The window also experiences loading due to the pressurization of the FC-75 coolant. This pressure which is ~270 kPa gauge (0.95 l/s) at the inlet is required to maintain the necessary flow velocity between the two windows.

2.6 General Atomics Distributed Window

The General Atomics (GA) distributed window illustrated in Figure 2-2 is a novel design approach to overcome some of the limitations of the double disk window. The distributed window approach uses sapphire as the window dielectric and water as the coolant. This is made possible by the use of a niobium louver structure in which the incident microwave beam is divided into many strips, each $< \lambda$ wide (λ being the free space wavelength). Each strip beam passes through a sapphire strip sealed between two niobium slats of the structure, each slat containing a water channel for efficient heat removal. The electric field is perpendicular to the slats. Since, with such an arrangement, significant wall currents flow on the sapphire-niobium interface, GA has developed a brazing technique for joining the sapphire strips to the niobium structure for which the measured skin losses are comparable to those of sapphire backed by machined copper. The advantage of the distributed window is the possibility of high cooling rates. This is due to the fact that water can be utilized as the cooling medium and the coolant pressure is not limited by the sapphire strength therefore permitting higher coolant flow rates.

The distributed window was analyzed using a 2D finite element model. The film coefficient was found using the turbulent flow theory, at 293 K coolant temperature and a flow rate of 0.000783 l/s per channel a film coefficient of 240 kW/m^2K was obtained. The film coefficient of the GA window is substantially higher than that of the double disk window due to the higher flow velocity and the water cooling medium. The analysis was performed by using one quarter of one fin section and taking advantage of the symmetry of the structure. The transient response and steady temperature rise were calculated. The obtained temperature distribution was then combined with the mechanical loading due to the coolant for a comprehensive stress

analysis. Cases were also considered where the window structure was prestressed at room temperature due to the high temperature brazing assembly operation.

2.7 Diamond Window

Diamond disks produced by chemical vapor deposition are increasingly becoming a viable microwave window material. It has become feasible to manufacture relatively large CVD diamond disks. Disks of up to 7.5 cm diameter and 1.2 mm thickness have been successfully grown. The loss tangent of the best material grade is $5 \cdot 10^{-5}$ at 145 GHz and 300 K [10]. According to Heidinger the loss tangent of diamond is inversely proportional to the frequency squared [10]. The thermal conductivity of diamond (1300 watt/mK) exceeds that of sapphire by a factor of ~30. The low loss tangent, high thermal conductivity combined with very high mechanical strength make CVD diamond a good microwave window candidate. The frequency scaling of the loss tangent make it an especially attractive material for high frequency gyrotrons as required by ITER.

A single disk edge cooled diamond window is illustrated in Figure 2-5. The window consists of a 5 to 7.5 cm diameter disk of which the outer 0.5 cm ring would act as a cooling fin. Such a window configuration was analyzed for 110, 145 and 170 GHz for both a 5 and 7.5 cm diameter.

The window was analyzed using an analytical approach assuming only radial heat transfer, for this case equation 2.7 simplifies to equation 2.35.

$$\frac{\partial^2 T}{\partial r^2} + \frac{1}{r}\frac{\partial T}{\partial r} + \frac{q(r)}{k_d} = 0 \tag{2.35}$$

where q(r) is the volumetric heat generation as a function of r, for this analysis a Gaussian and a ring distribution were considered. For a Gaussian distribution the temperature profile must be evaluated using numerical calculation, for a ring distribution of the form given in equation 2.36 the temperature distribution is given by the analytic expression in equation 2.38.

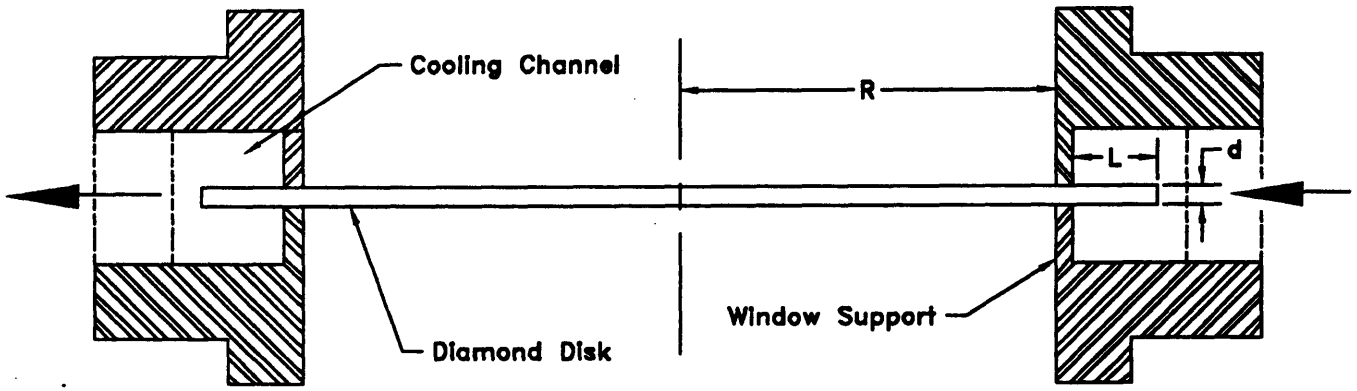

Figure 2-5: Schematic of Single Disk Edge Cooled Diamond Window

$$q(r) = Q(ar^3 + br^2 + cr + d) \tag{2.36}$$

$$T(r) = \left(\frac{Q}{k}\left(\frac{a}{25}(R^5 - r^5) + \frac{b}{16}(R^4 - r^4) + \frac{c}{9}(R^3 - r^3) + \frac{d}{4}(R^2 - r^2)\right)\right) + T_{max} \tag{2.37}$$

$$0 \leq r \leq R$$

where R is the effective window radius and T_{max} is given by equation 2.38. This solution assumes a constant temperature boundary condition T_{max}, this temperature can be evaluated by calculating the temperature distribution and rise of the cooled edge of the diamond disk. The maximum temperature of the annular fin is given by equation 2.38.

$$T_{max} = \frac{\cosh(mL) + \frac{h}{mk}\sinh(mL)}{\sinh(mL) + \frac{h}{mk}\cosh(mL)} \frac{Q_{tot}}{M} \tag{2.38}$$

where L is the length of the fin, k the thermal conductivity of the diamond, h the film coefficient and Q_{tot} the total heat deposited in the window. The dimensionless

parameters m and M are given by equation 2.39 and 2.40.

$$m = \sqrt{\frac{hP}{kA}} \tag{2.39}$$

$$M = \sqrt{hPkA} \tag{2.40}$$

$$\begin{aligned} A &= (R + \frac{L}{2})d \\ P &= 2(R + \frac{L}{2}) \end{aligned} \tag{2.41}$$

where A is the average cross-sectional area, P is the average azimuthal perimeter of the annular fin and d is the thickness of the diamond disk. The temperature distribution across the cooling ring is given by equation 2.43 [13].

$$\begin{aligned} T(r) &= \frac{\cosh(m(L+R-r)) + \frac{h}{mk}\sinh((m(L+R-r))}{\cosh(mL) + \frac{h}{mk}\sinh(mL)} T_{max} \\ & \\ & R \leq r \leq R + L \end{aligned} \tag{2.42}$$

For a flow rate of 1 l/s and a cooling passage of 6 by 6 mm, the film coefficient was found to be 52.5 kW/m^{2}K.

A 2D finite element analysis was also employed to calculate the temperature rise and transient response of the diamond window. Using the obtained temperature distribution and mechanical loading due to coolant and atmospheric pressure, the thermal and mechanical stresses were calculated.

Chapter 3

Experimental Measurement

3.1 Introduction

In conjunction with Varian Associates in Palo Alto, Ca temperature measurements were conducted of a double disk sapphire output window on a 500 kW long pulse gyrotron. These experiments were carried out to validate the theory for the temperature response of the double disk window and to establish actual values for the loss tangent, its temperature dependence and the film coefficient.

3.2 Temperature Measurements

Temperature measurements of gyrotron windows in actual operation are made difficult by the presence of several hundred kilowatts passing through the window [11, 12]. This makes direct contact temperature measurements virtually impossible. Alternatives are the use of infrared cameras, ultrasonic units or laser interferometers, which measure the thermal expansion of the window. For infrared temperature measurements of sapphire, long-wave infrared detectors must be used, as sapphire only has a strong thermal emission in the long wave portion of the infrared spectrum (8-12 μm). For these temperature measurements a long wave infrared camera (Agema Thermovision 780) was used, which was shielded from the microwave beam by placing it behind a microwave filter which was incorporated into an elbow mirror. The microwave filter

is composed of a number of small circular holes whose radius is below cutoff of the microwaves. The camera setup is shown in Figure 3-1.

The camera was placed 3° off the window axis to prevent microwaves from leaking into the camera and to prevent any spurious reflections of the lens back to the window, which would introduce noise into the camera image.

Microwave power intensity distributions were obtained by using shorter pulses (~2 ms) and placing a piece of absorbant paper between the camera and the window. This allowed a recording of the actual microwave pattern under actual operating conditions. Such patterns were obtained directly at the window and at the end of the output waveguide. Figure 3-2 shows the microwave intensity pattern at the end of the 15 cm long window output 10.16 cm diameter waveguide.

The intensity profile at the end of the waveguide exhibits a peaking factor of 2.7 with one distinct hotspot and croissant shaped secondary hotspot. The pattern at the window. shown in Figure 3-3, exhibits one very pronounced hotspot at the same location, but the remainder of the window pattern differs. The rest of the window is approximately at an equal intensity level with a small peak at the center. The peaking factor for this pattern is only 1.7. Cold tests conducted of the mode converter with a low-power source are in good agreement with the intensity pattern recorded at the end of the waveguide. The cold test peaking factor was between 2.7 and 3.3, which agrees well with the waveguide intensity pattern.

The discrepancy between the two patterns can be explained by reflections on the waveguide in the case of the window intensity profile. Infrared radiation in the 8-12 μm range emitted by the hot spot, bounces around in the smooth waveguide, causing part of it to be reflected into the camera. The hotspot therefore raises the apparent background temperature and thereby reduces the peaking factor as well as introducing a phantom peak at the center of the window. Since the infrared radiation emitted is proportional to the temperature to the fourth power a low level of reflection can cause considerable distortion of the camera image. This provides a possible explanation of the low peaking factor of the window intensity pattern.

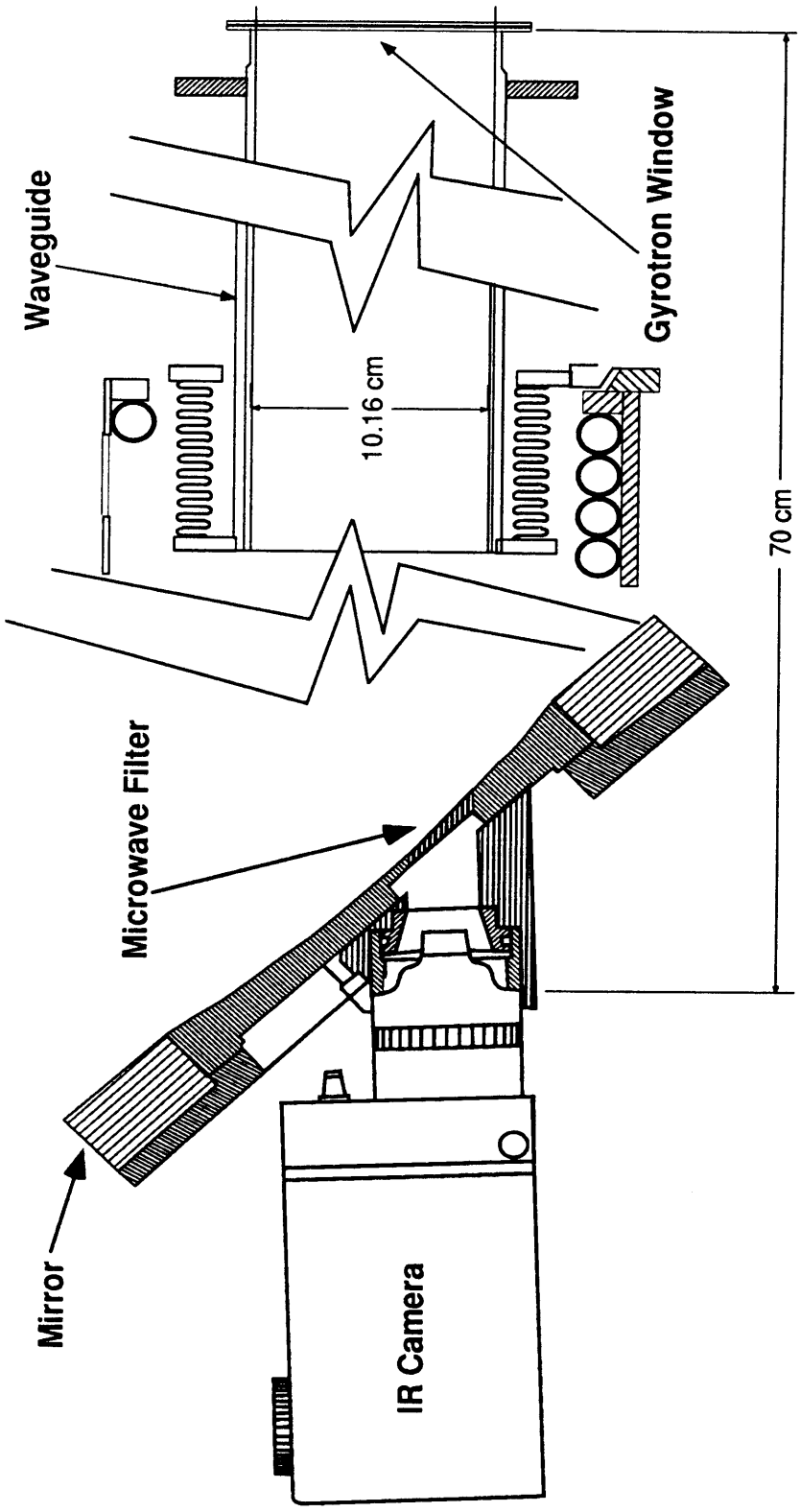

Figure 3-1: Experimental Infrared Camera setup

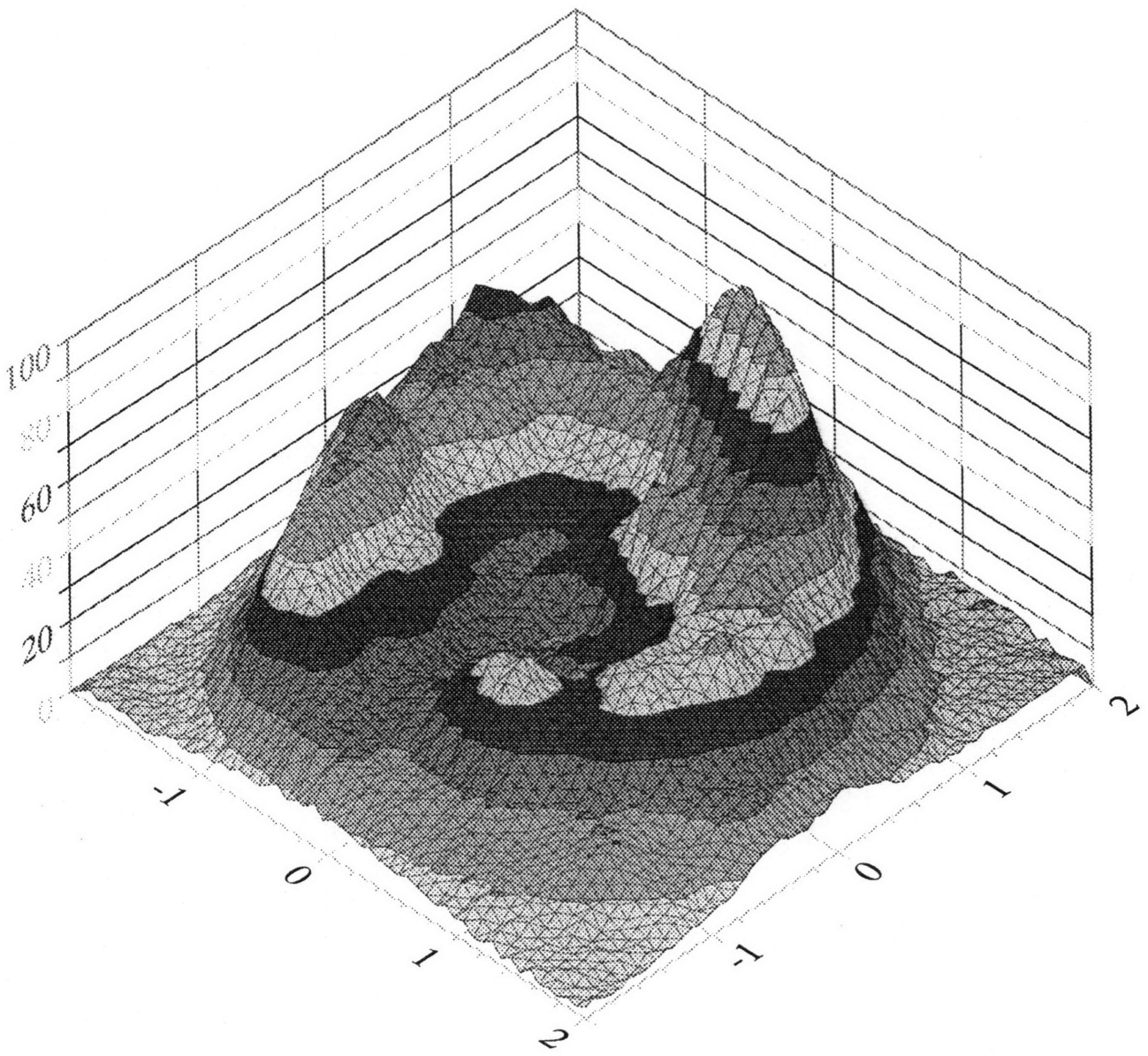

Figure 3-2: Normalized Intensity profile at the end of the Waveguide measured with absorbing paper (Dimensions in inches)

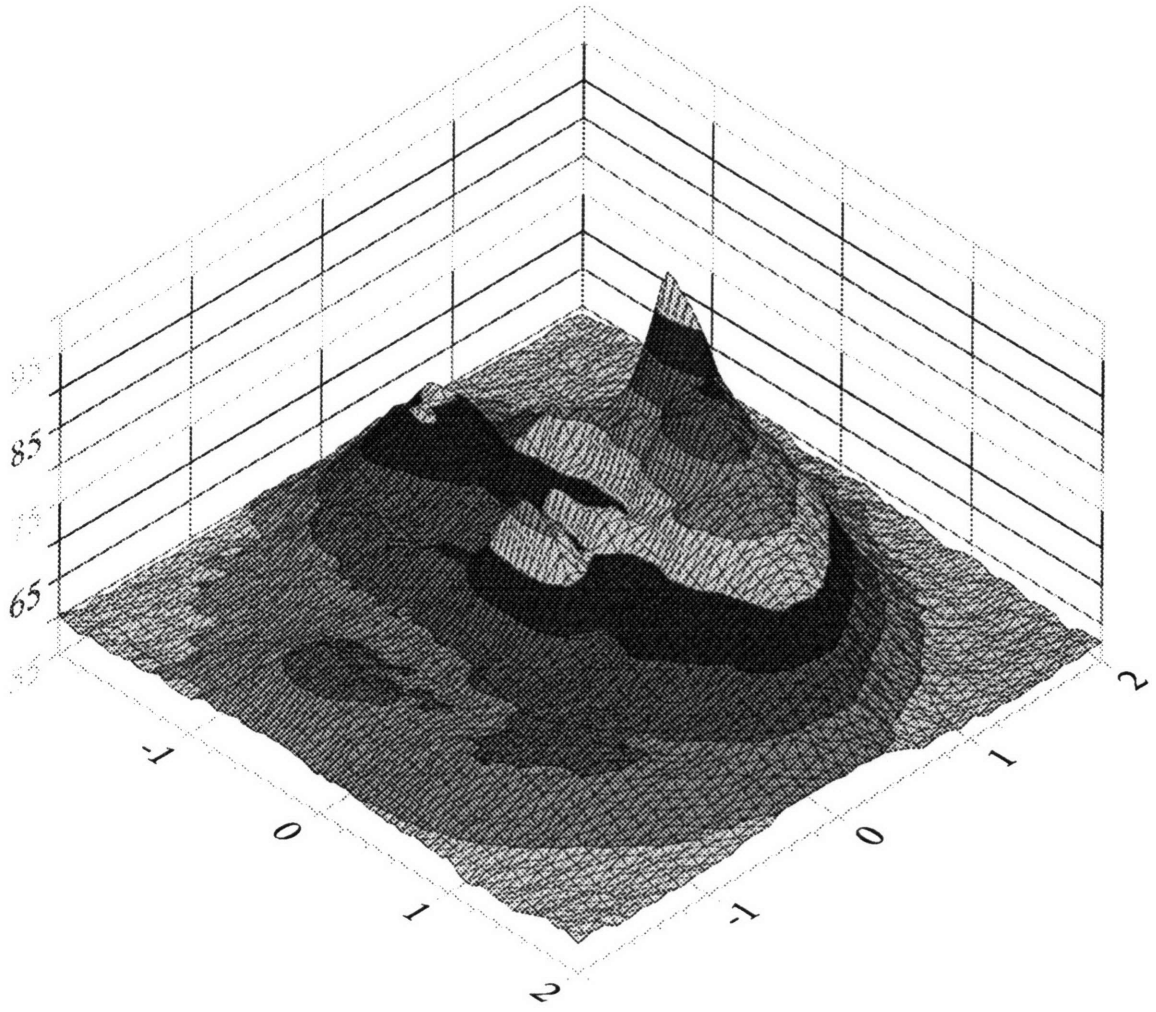

Figure 3-3: Normalized Intensity profile at the Window measured with teflon backed absorbing paper for a 200 kW, 2 ms pulse

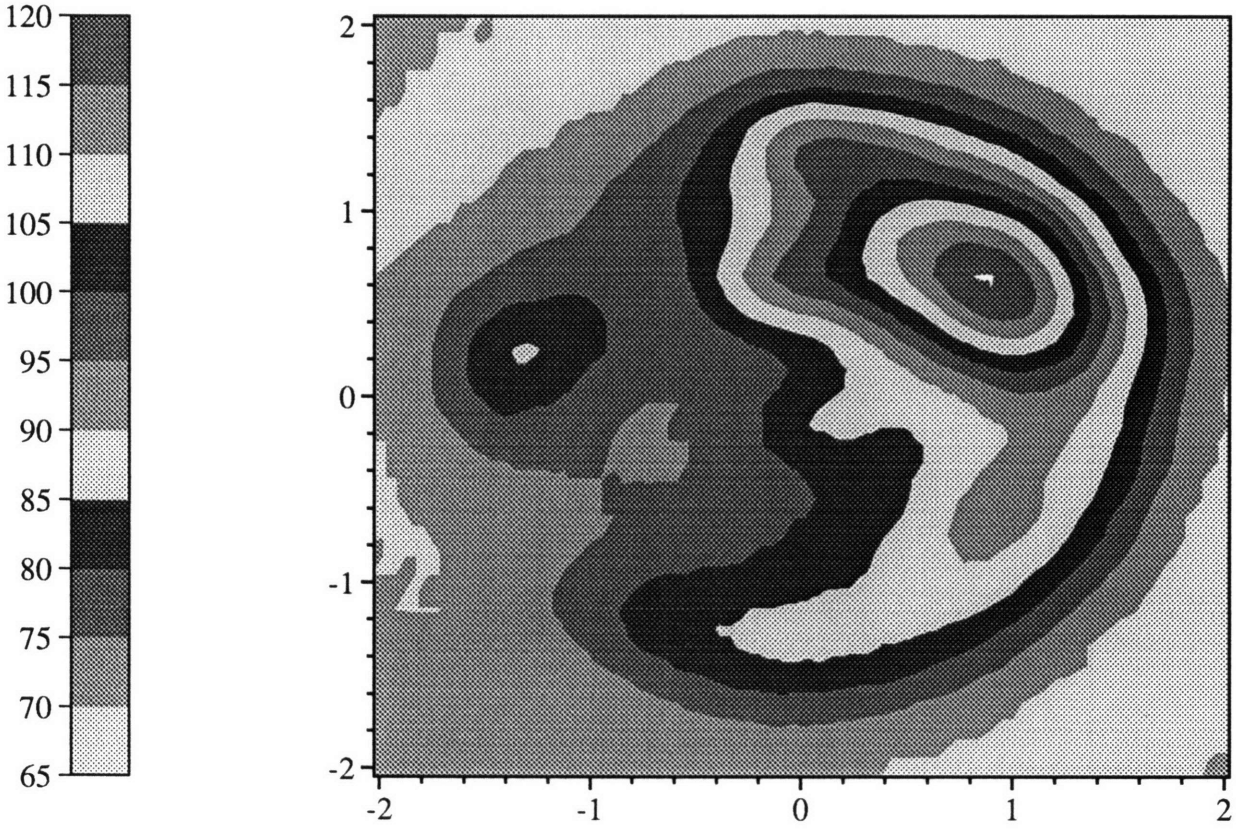

Figure 3-4: Equilibrium Temperature Rise for 400 kW 6 second pulse in K (Dimensions in inches)

In the window temperature measurements the distribution is smoothed due to 3D thermal conduction effects, which are particularly relevant for a highly asymmetric distribution as recorded here. The peaking factor of the intensity pattern should therefore be higher especially when compared to a typical window pattern, as shown in Figure 3-4, where the peaking factor is 1.7. This leads to the conclusion that the window patterns and sapphire temperature measurements have a considerable amount of noise associated with them. The sapphire temperature measurements are equally affected by the reflection, therefore these images are inaccurate apart from the primary hotspot which is less sensitive to noise due to its significant higher signal level. The hot spot was therefore utilized to extract the loss tangent, its temperature dependence and the film coefficient.

The transient response for the peak temperature location for 350, 400 and 530 kW pulse is show in Figure 3-5. The 350 and 400 kW pulses reach steady state after $\sim$4 seconds, while the 500 kW, 2 second pulse does not show any sign of reaching steady

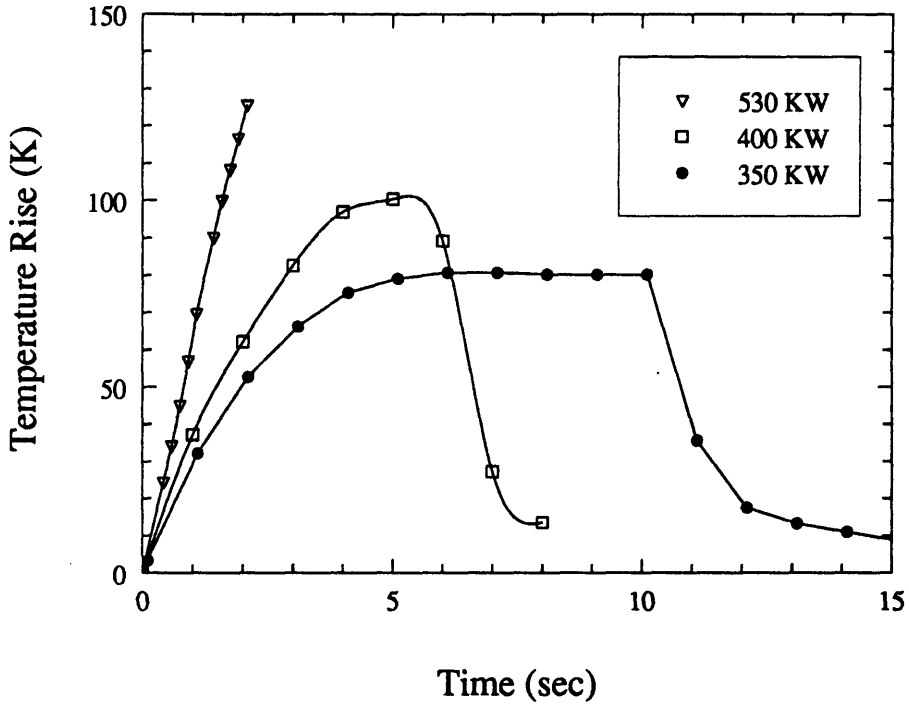

Figure 3-5: Transient Temperature Response for a Coolant Flowrate of 0.85 l/s

state, it exhibits thermal runaway and illustrates the strong temperature dependence of the loss tangent. The film coefficient of the window structure can be determined from the fall time of the sapphire window after the microwave beam has ended. This portion of the response is simply the cooling of the sapphire from an initial temperature. It is therefore independent of the loss tangent and its temperature dependence and is dictated by the film coefficient. The film coefficient was determined to be 5.8 kW/m^{2}K at a nominal flow rate of 0.85 l/s and a bulk temperature of 293 K. This compares to a theoretical film coefficient of 6.7 kW/m^{2}K for the same parameters. Utilizing this value for the film coefficient a loss tangent as given by equation 3.1 was established.

$$tan\delta = 1.3 \cdot 10^{-4} \left(\frac{T}{300\text{K}} \right)^{1.7} \tag{3.1}$$

Figure 3-6 shows temperature measurements for a 350 kW, 10 second pulse for the first four seconds at a one second interval. The temperature pattern remains the same

over the duration of the pulse.

3.3 Flow Characterization Experiments

To establish the film coefficient for the window structure and its dependence on the flow rate, various flow characterization experiments were conducted with a 200 kW, 7 second pulse. The flow rate was varied between 0.47 and 0.85 l/s in increments of 0.063 l/s and at a coolant bulk temperature of 293 K. Sample transient responses are shown in Figure 3-8. The bulk coolant temperature was varied between 284 and 295 K at a flowrate of 0.85 l/s. In addition the flow direction of the FC-75 was altered in order to study the effect of the hot spot location relative to the flow pattern on the overall window temperature rise. The inlet and outlet coolant pressure were recorded over the range of flowrates. These results compared very well with the theoretical predicted pressure drop Figure 3-7.

The temperature rise after 7 seconds versus the coolant flow rate is shown in Figure 3-9. The thermal runaway effect is clearly visible for flowrates of less than 0.6 l/s in Figure 3-8. The window structure exhibits a high sensitivity to the flow rate, as the flow rate decreases the temperature increases dramatically. The theoretical prediction from the turbulent flow model and subsequent finite element analysis does not exhibit the same sensitivity. The experimental film coefficient is significantly more sensitive to the flow rate at low flow velocities than the model predicts. The theoretical curve and experimental results are shown in Figure 3-9. As the flow rate decreases, the flow enters the transitional regime between being turbulent and laminar causing a significant reduction in the film coefficient and therefore a higher temperature rise and a longer rise time.

Reversing the flow direction had a dramatic effect on the temperature rise of the window. With the hot spot located next to the flow inlet the temperature rose dramatically at lower flow rates relative to the normal flow direction. This effect can be explained by the absence of a perturber in the input baffle for the reversed flow direction. The perturber is designed to induce additional turbulence into the flow and

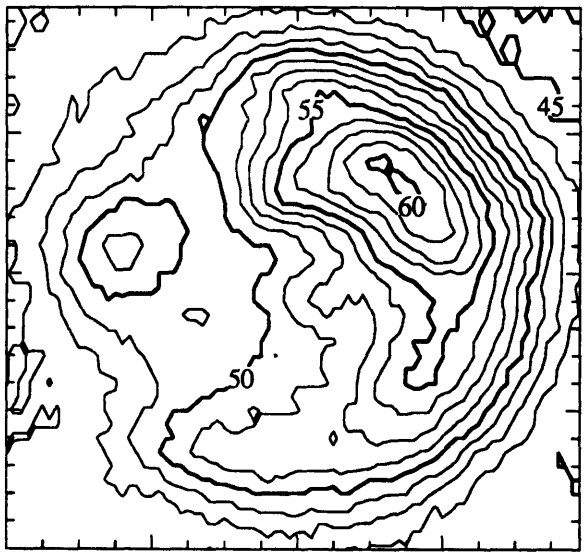

1 sec

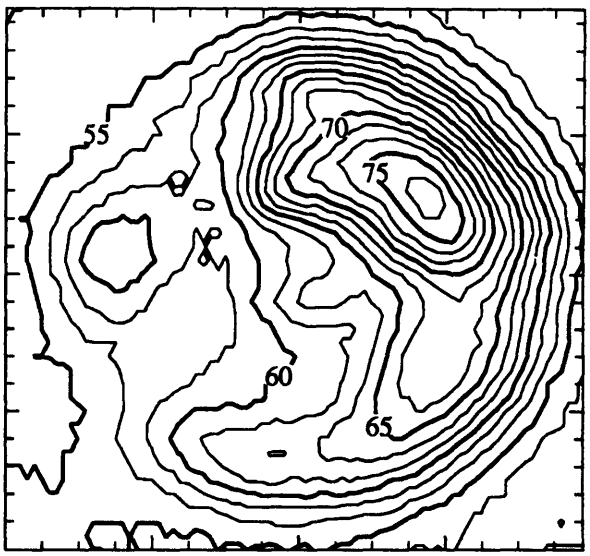

2 sec

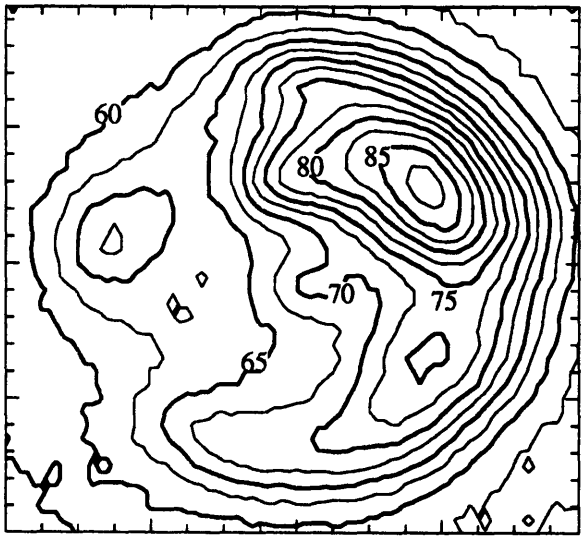

3 sec

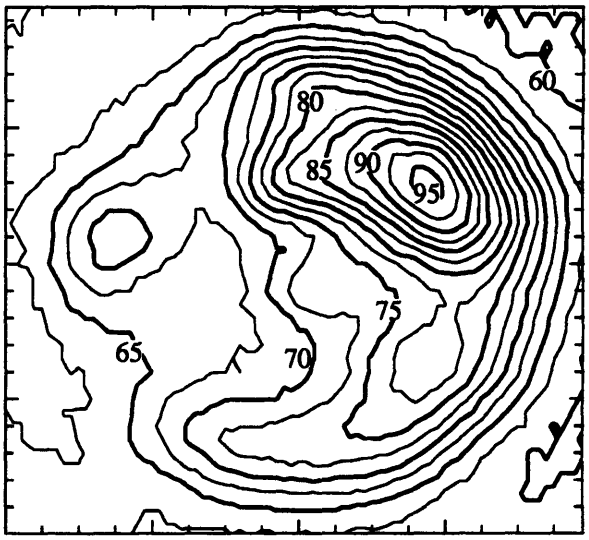

4 sec

Figure 3-6: IR camera measurements for a 350 kW, 10 second pulse

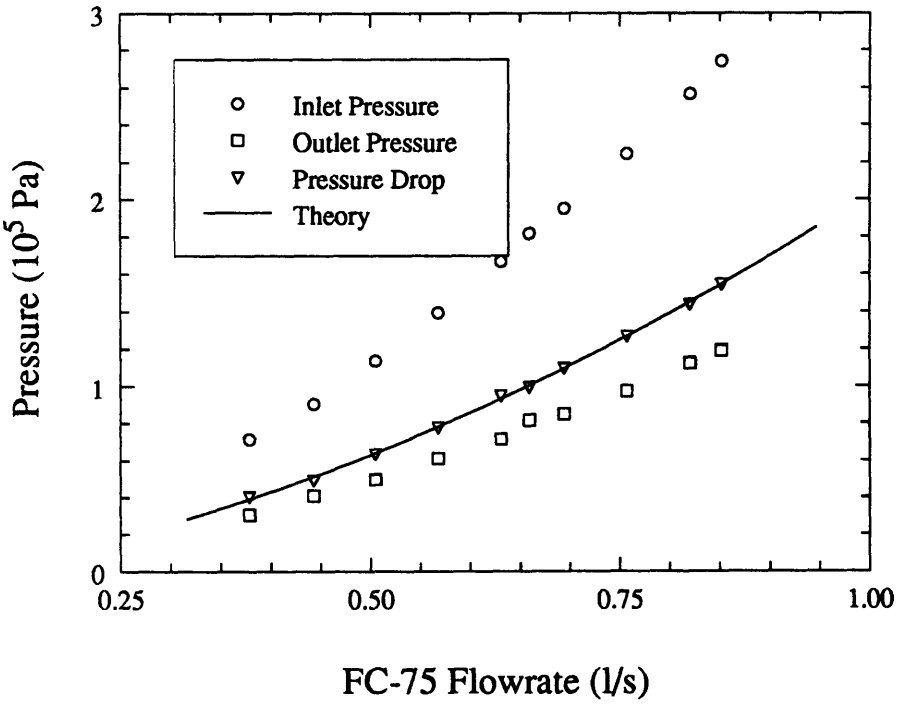

Figure 3-7: Coolant Pressure vs Flowrate of Double Disk Window

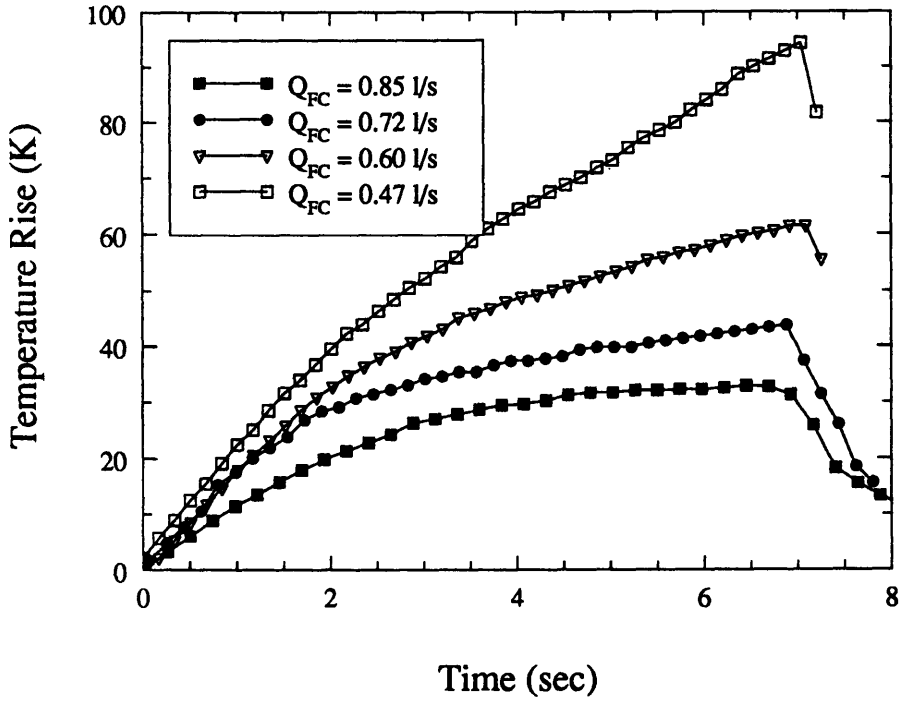

Figure 3-8: Transient Temperature Responses for Flow Rates between 0.47 and 0.85 l/s at 200 kW

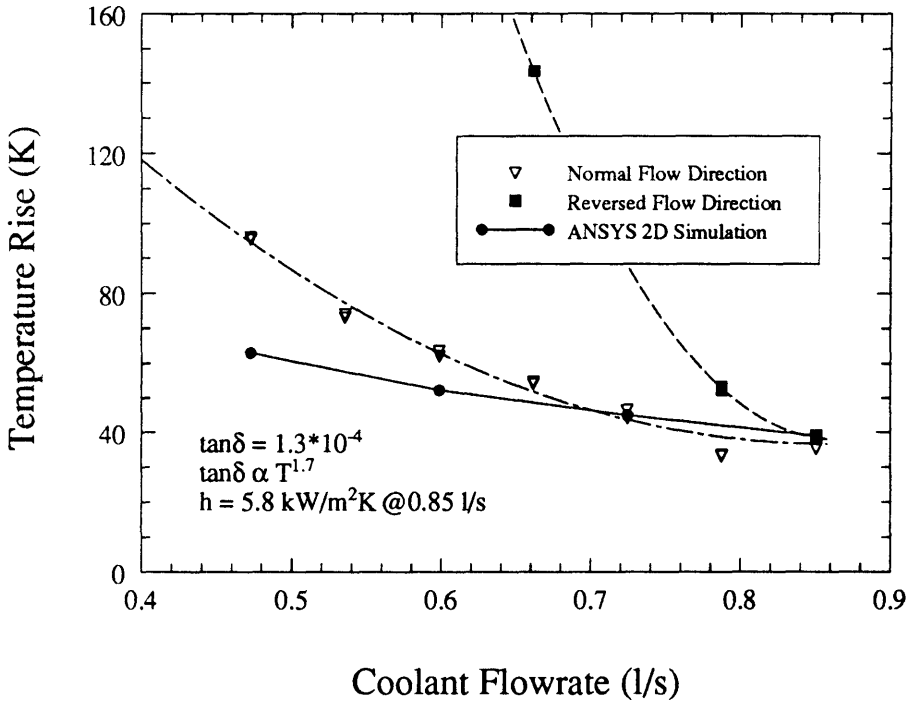

Figure 3-9: Temperature Rise after 7 seconds versus Flow Rate for 200 KW, 7 second pulses

prevent flow separation from the walls. At lower flow rates as the Reynolds number decreases, the perturber effect becomes more critical in maintaining the turbulence of the flow.

Chapter 4

Analysis

4.1 Introduction

Thermal and mechanical finite element analyses of the three window types were conducted. For the case of the double disk window the thermal calculations were compared to the experimental temperature data obtained from the double disk sapphire window, Chapter 3.

4.2 Double Disk Window

The sapphire double disk window was analyzed utilizing analytical and finite element solutions. The theoretical temperature rise and response were compared with the experimental temperature data, Chapter 3. The effects of the peaking factor on the thermal performance of the window was investigated. The stress and thermal levels were analyzed for variations in the window dimensions. Since both disks experience an identical intensity distribution and film coefficient only one of the disks needed to be analyzed for its thermal characteristics.

4.2.1 Thermal Analysis

The double disk window was initially analyzed using a 1D analytical solution. Such 1D solutions are sought at the location of highest power intensity. Since all the heat

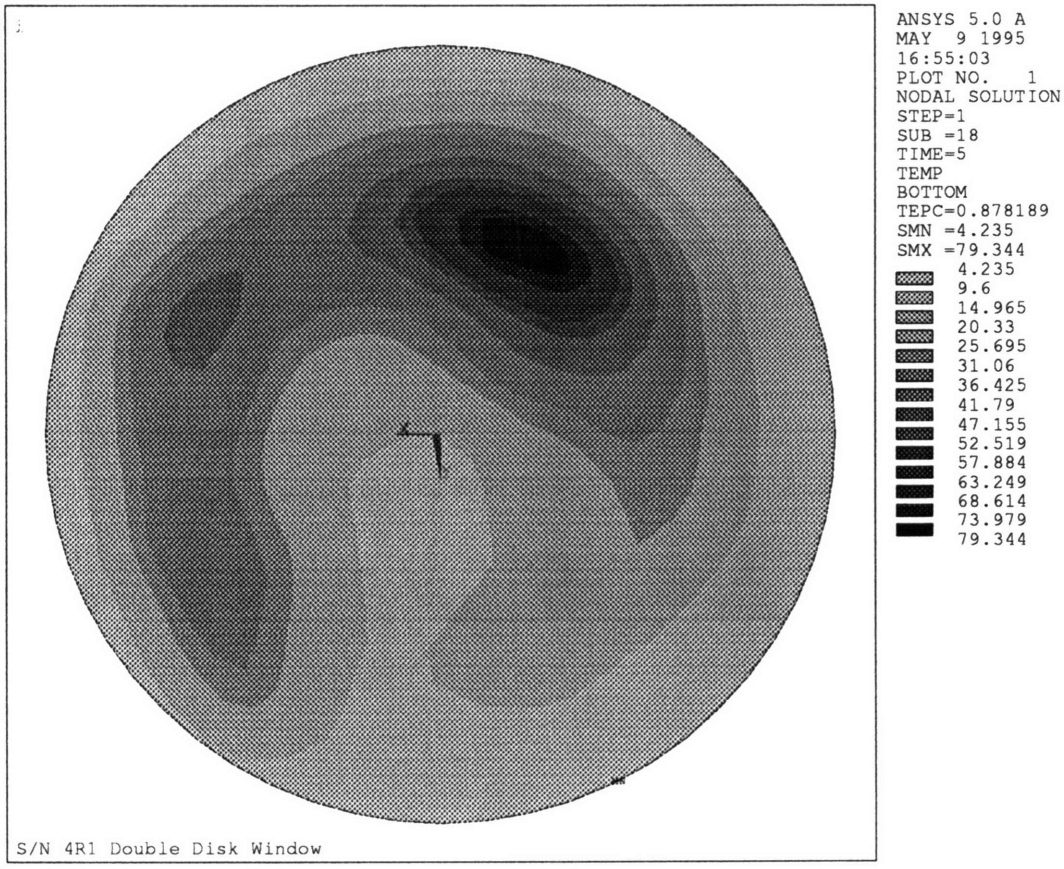

Figure 4-1: Finite Element Simulation for Temperature Rise with measured Intensity Distribution for 350 kW (K)

flow out of the window is assumed to be out of the cooled face, the high aspect ratio (L/R) justifies a 1D analytical solution. For an axisymmetric intensity profile 1D numerical simulations overestimate the temperature rise by approximately 13%. For a non-axisymmetric distribution the error increases, due to azimuthal heat conduction. For the intensity distribution recorded at the end of the waveguide the error is approximately 25%.

In order to compare the experimental temperature rise with the theory a 3D thermal finite element analysis was performed with the recorded intensity profile. The measured intensity pattern at the end of the waveguide was used as a heat generation distribution input into a 3D thermal finite element model of one of the sapphire window disks, the resultant temperature distribution for the waveguide aperture (10.16 cm) of the window is show in Figure 4-1 The experimental equilibrium temperature rise for a 350 kW, 10 second pulse is shown in Figure 4-2.

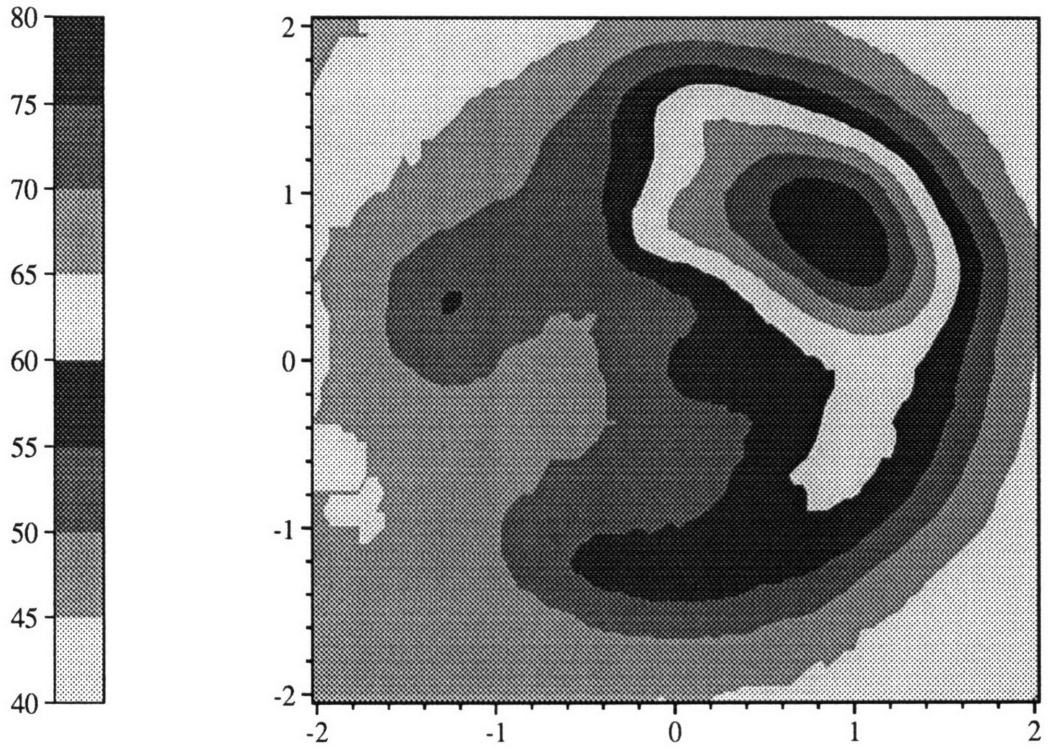

Figure 4-2: Experimental Temperature Rise for 350 kW (K) Dimensions in inches

The experimental temperature distribution exhibits a significantly larger background temperature, the minimum temperature rise on the window is 45 K. The center of the window is also at significantly higher temperature than in the 3D finite element simulation. The edges of the camera image indicate a temperature rise of approximately 40 K, while in fact there are cooled waveguide components around the output sapphire window whose actual temperature rise, monitored with thermocouples, is very small. The high temperature rise in these outer regions of the camera image indicates that infrared radiation from the hotspot is reflected off the waveguide into the camera, which causes the background temperature and lower temperature regions of the window to have a higher signal level and thereby resulting in a higher apparent temperature of the low temperature regions. It should be noted that the hot spots in both cases are at the same location and they are of equal magnitude.

The steady state temperature rise versus power was obtained using a 3D simulation, the results of which are shown in Figure 4-3. The maximum allowable temperature rise is dictated by the boiling point of the FC-75 coolant. For an initial

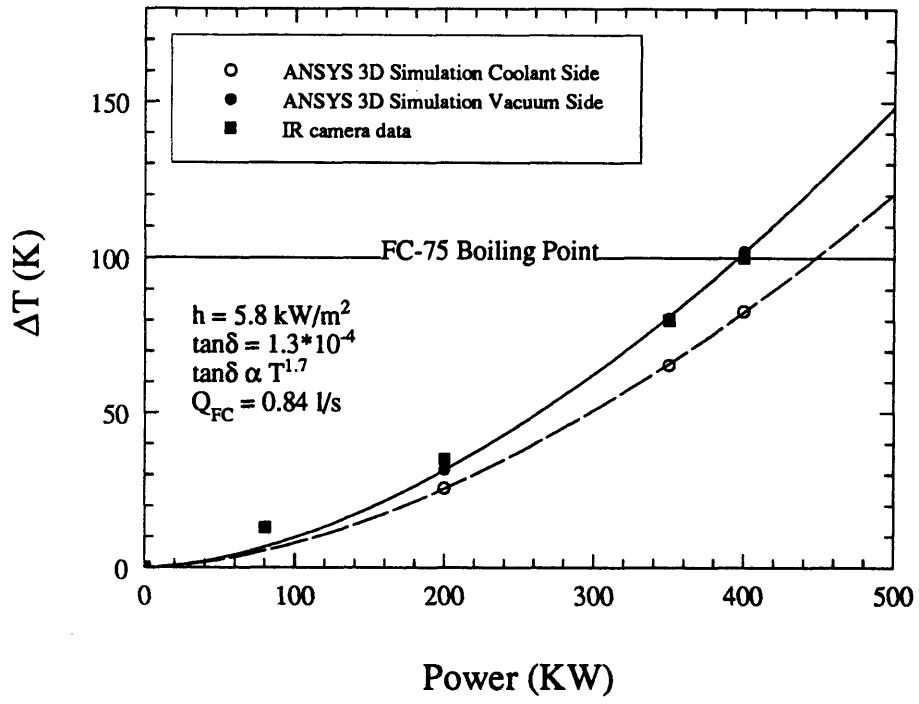

Figure 4-3: Double Disk Window Equilibrium Temperature versus Power

coolant temperature of 293K the maximum power handling capability of the window is limited to 450 kW with the present pattern. Using an axisymmetric pattern the temperature curve is shifted down slightly due to the lowering of the peaking factor. In order to increase the power handling capability of the present window the microwave beam has to become more symmetric and the peaking factor needs to be reduced. Figure 4-4 illustrates the power versus peaking factor tradeoff, for a peaking factor of 2 the maximum power is 550 kW. The thermal simulations and experimental results illustrate that the present double disk window is limited by thermal runaway.

The transient response was also investigated, Figure 4-5, illustrates the theoretical and experimental hot spot temperature rise for a 350 kW pulse. For this 3D finite element simulation the heat generation rate in the window was adjusted at each timestep to account for the temperature dependence of the loss tangent. The experimental temperature rise and simulation are in very good agreement. The finite element simulation for the temperature drop off is in very good agreement for

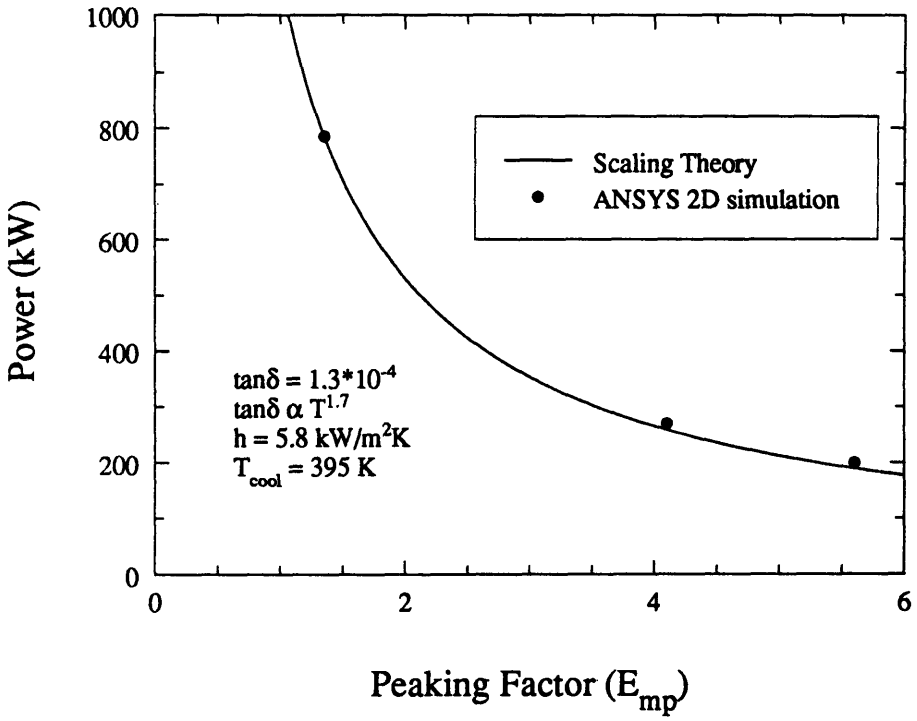

Figure 4-4: Maximum Power Transmission Capacity versus Peaking Factor of Double Disk Window for a Coolant Side Temperature of 395 K

the first two seconds, which represents 75% of the effective temperature drop. All transient temperature drops, regardless of the initial temperature, display this slow transient behaviour for the last 20 K, the discrepancy can therefore be attributed to external infrared radiation sources. The theory utilized for the computation of the film coefficient overestimates it by 15%. The discrepancy of the film coefficient between theory and experiment can be attributed in part to the large aspect ratio of the cooling channel, this could lead to an overestimate of the theoretical Reynolds and Nusselt numbers and subsequently to a higher theoretical film coefficient. At 0.85 l/s the theoretical Reynolds number is $\sim$ 17,000, well over the $\geq$ 10,000 criterion for fully developed turbulent flow. The theory overestimates the Reynolds number and thereby the film coefficient. Therefore as the flow rate decreases, the flow enters the transitional regime between being turbulent and laminar causing a significant reduction in the film coefficient. The theory therefore predicts a substantially lower temperature rise for lower flow rates, due to the overestimation of the film coefficient,

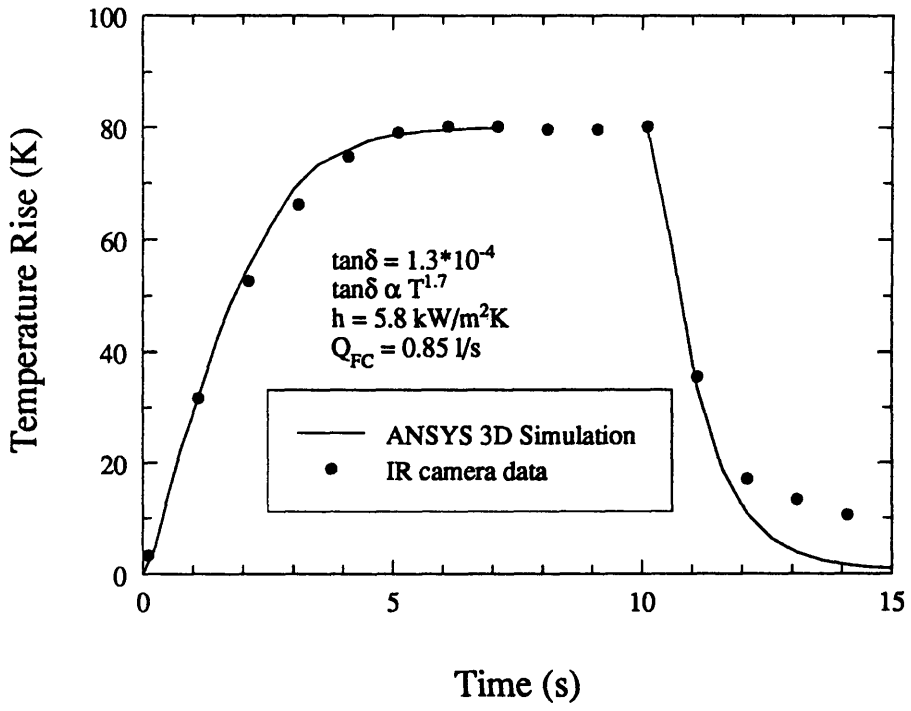

Figure 4-5: Transient Response of Double Disk Window

as is illustrated in Figure 3-9.

The experimentally measured loss tangent of $1.3 \cdot 10^{-4}$ at 300 K with a temperature dependence of $T^{1.7}$, compares well with Heidingers results. The temperature dependence of the loss tangent is slightly higher 1.7 versus 1.46 and the room temperature loss tangent (300 K) is $1.3 \cdot 10^{-4}$ versus $1.5 \cdot 10^{-4}$. The difference is attributable to different material grades and experimental error, as well as, to the fact that Heidinger's highest temperature data point is at 340 K. The Japanese Atomic Energy Research Institute (JAERI) estimated a sapphire loss tangent of $1.5 - 2.0 \cdot 10^{-4}$ from the short pulse temperature rise gradient [14].

The effect of varying the window dimensions is illustrated in Figure 4-6. A larger window decreases the intensity per unit area, the intensity is inversely proportional to the radius squared. As the window radius is decreased the film coefficient for a constant flow rate is also decreased, as the cross sectional area of the flow channel increases and the mean flow velocity is diminished. The film coefficient is inversely proportional to approximately $R^{0.8}$. An increase in the window thickness raises the

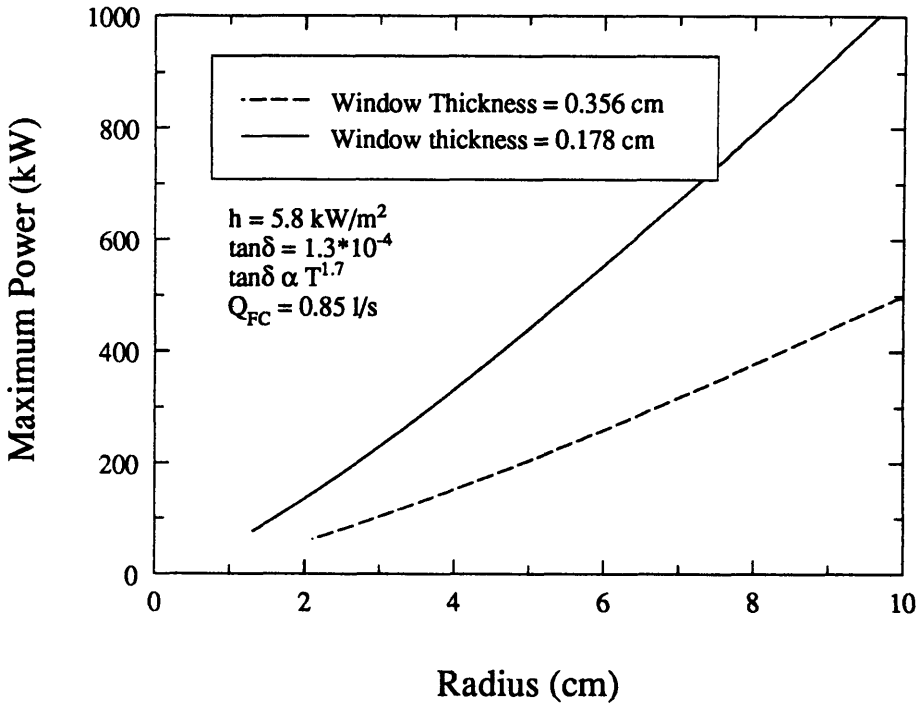

Figure 4-6: Effects of window dimension variation on Maximum Power Level of Double Disk Sapphire Window for a coolant side temperature of 395 K

total heat generated in the window and thereby is detrimental to the window's thermal performance. Figure 4-6 illustrates that the maximum acceptable power level decreases substantially when the window thickness is increased.

4.2.2 Mechanical Analysis

The finite element stress analysis of the sapphire double disk window was performed on the inner disk. This disk is subjected to a higher pressure loading due to the internal vacuum of the gyrotron tube. In the case of an axisymmetric temperature distribution, advantage of symmetry can be taken and only half of the disk needs to be analyzed.

The performed 3D stress analysis indicates that the double disk is operating close to its maximum stress level. The largest stress contribution comes from the mechanical loading of the disks by the coolant pressure. An outer support ring can be utilized to constrain the thermal expansion by compressively loading the window [7].

The tensile stresses are then distributed over a greater portion of the window and the peak stress is reduced. The large mechanical tensile stresses are compensated to a limited extent by the thermal stresses which arise during gyrotron operation.

Reliable estimates of the window stresses therefore require the combination of the mechanical and thermal loading. The maximum radial tensile stress of 156 MPa occurs near the window support. The maximum compressive stress is 257 MPa. Contour plots of the tangential and radial stresses in the window assembly for 400 kW and 0.85 l/s are shown in Figure 4-8 and 4-9. The coolant flow is in the negative x-direction. The stress distribution is not significantly affected by the temperature profile, i.e. axisymmetric distribution versus the experimentally determined distribution, as most of the stresses are of mechanical nature.

The maximum stresses generated in the double disk window as a function of window dimensions are shown in Figure 4-7. While the thermal performance of the window is improved by enlarging the window, the mechanical stresses increase dramatically. An increase in the window thickness thickness to reduce the mechanical stresses in the window would cause a substantial drop in thermal performance, a window thickness increase is therefore not a viable option. An increase of the window waveguide aperture radius to 5.75 cm would increase the maximum power transmission capacity of the window from 450 to 525 kW for the present window pattern, while keeping the mechanical stresses to a reasonable level, i.e a maximum compressive stress of 300 MPa and a maximum tensile stress of 185 MPa.

Stress failure in sapphire occurs as a result of the formation and propagation of cracks in the crystal. Through surface treatments the cracks on the crystal surface can be reduced, elevating the mechanical strength of the material [2]. By utilizing such superpolished sapphire disks, the radius of the double disk window could be increased thereby raising the power handling capacity.

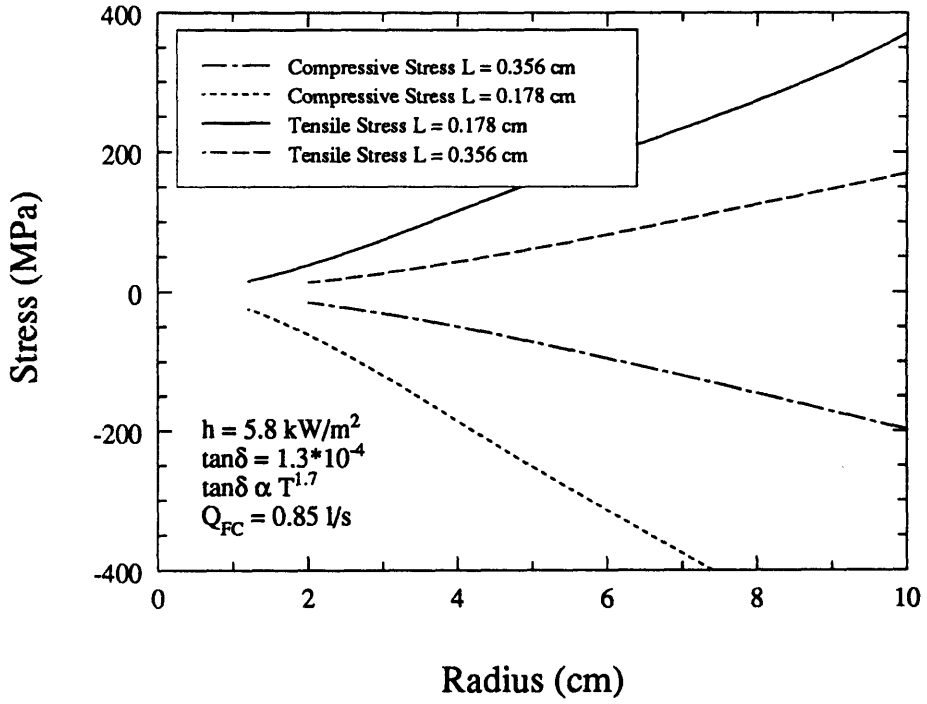

Figure 4-7: Effects of window dimension variation on Stresses of Double Disk Window for a coolant side temperature of 395 K

4.3 General Atomics Distributed Window

The distributed window was analyzed for thermal and mechanical performance using a 2D finite element analysis. By taking advantage of the symmetry in the structure only a quarter of one of the the niobium fin sections needed to be analyzed. The section with the highest microwave power impinging on it was considered in this case.

4.3.1 Thermal Analysis

The General Atomics distributed window was thermally analyzed for a HE_{11} mode at a 1 MW power level. The relevant heat fluxes and heat generation rates for these parameters are illustrated in Figure 4-10. The section experiencing the maximum intensity RF power was analyzed. The high ohmic losses along the sapphire niobium braze should be noted, these present a major contribution to the total temperature rise in the window.

The fin tip reaches a maximum temperature rise of 50 K due to the high ohmic

Figure 4-8: Radial Stresses in the Double Disk Window for 400 kW and 0.85 l/s coolant flowrate in MPa (1: vacuum side, 2: coolant side)

Figure 4-9: Tangential Stresses in the Double Disk Window for 400 kW and 0.85 l/s coolant flowrate in MPa (1: vacuum side, 2: coolant side)

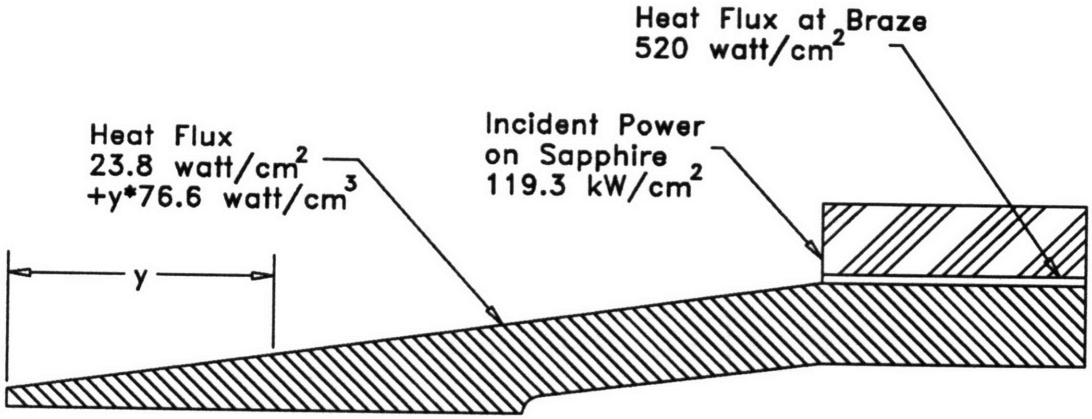

Figure 4-10: Heat Fluxes on Distributed Window for 1 MW [17]

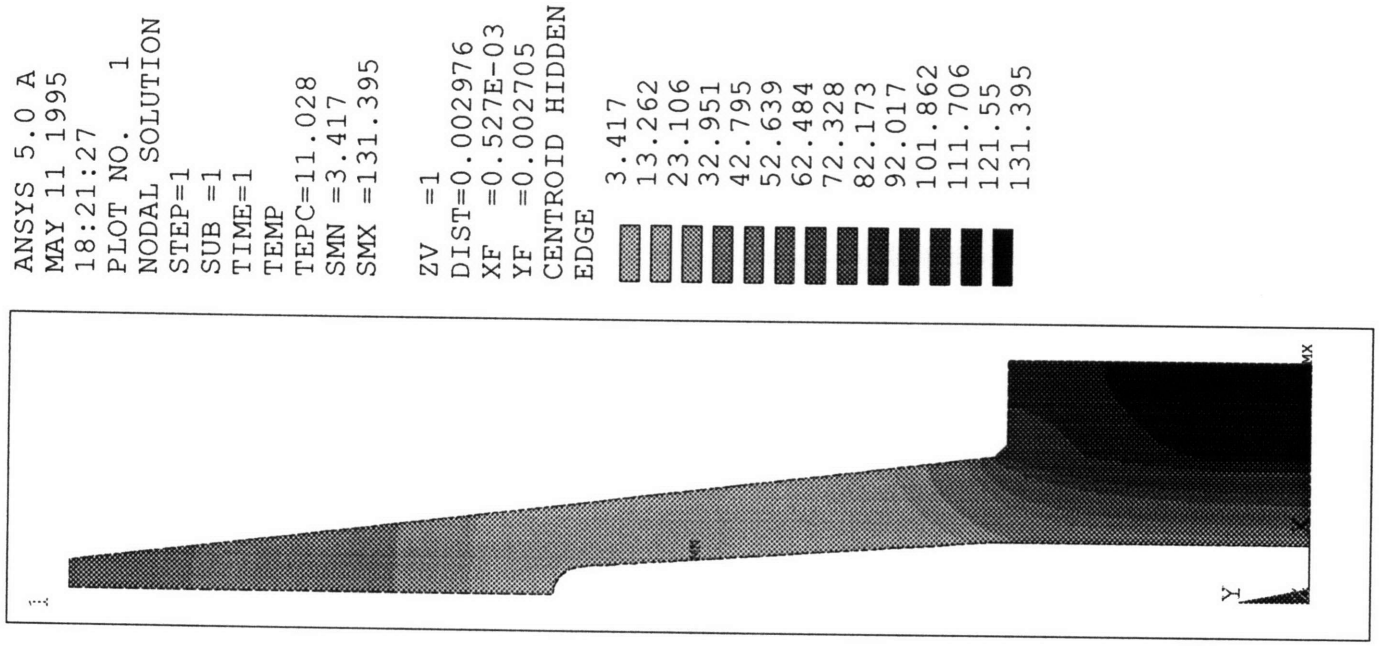

Figure 4-11: Equilibrium Temperature Rise of Distributed Window for 1 MW in the HE_{11} mode

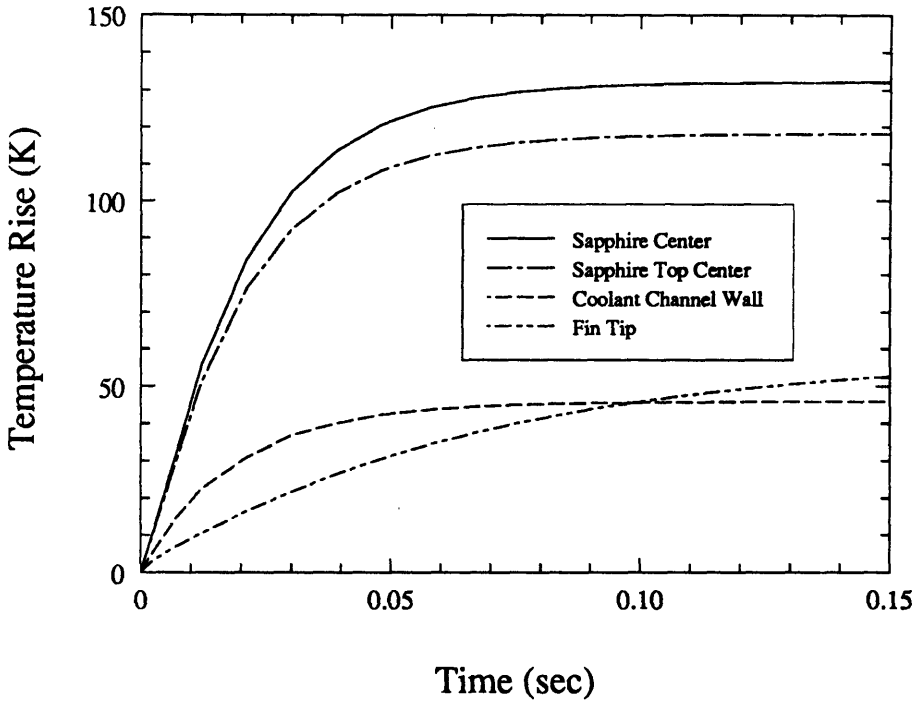

Figure 4-12: Transient Response of the Distributed Window for 1 MW

losses along the metal surface and the long thermal conduction path from the tip to the cooling channel. The cooling channel is limited in its height by the width of the EDM wire used in the machining process. The maximum temperature rise of 131.4 K is at the center of the sapphire strip. The thermal simulation was also analyzed for its thermal transient response. The window has a 98% rise time of .11 seconds, this short rise time is due to the high film coefficient in the cooling channels and the short thermal path length, the distance between the sapphire center and the cooling channel is only 0.72 mm. A sample transient response for the 110 GHz window is shown in Figure 4-12.

4.3.2 Mechanical Analysis

The stresses in the window structure were obtained by combining the temperature distribution obtained in the thermal analysis with the mechanical loading it is subjected to by the coolant pressure. For the stress analysis two cases were considered.

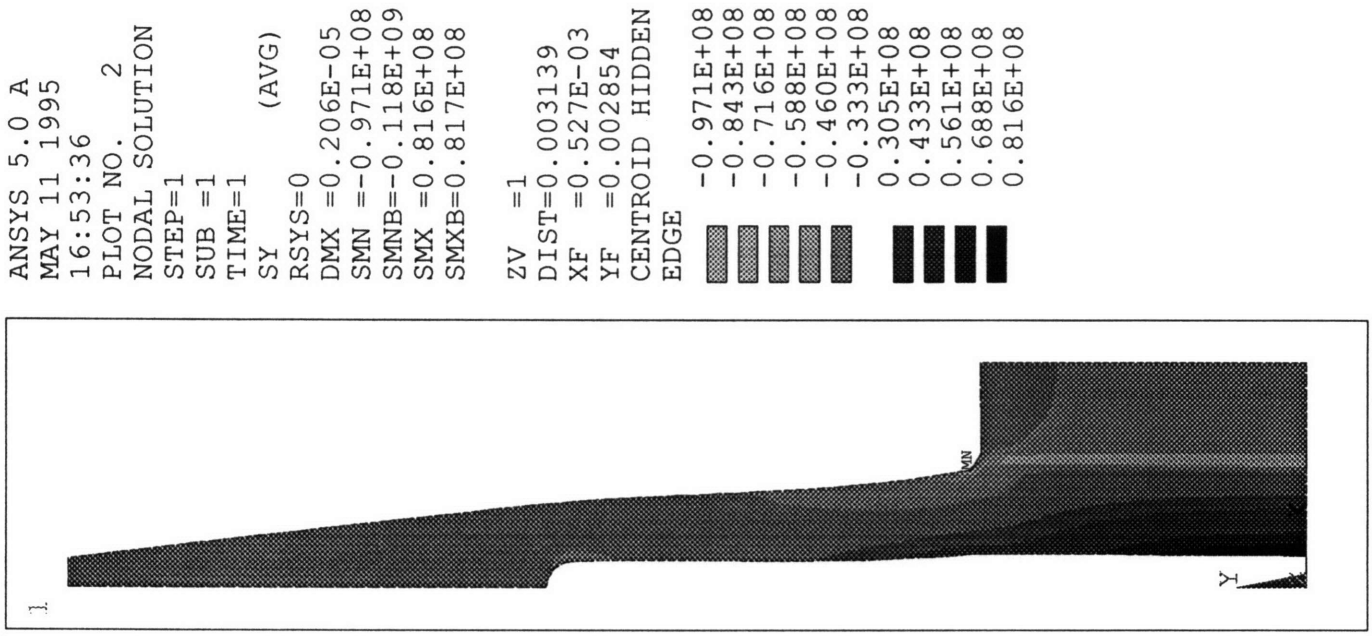

Figure 4-13: Stress Analysis of Distributed Window for 1 MW Y-axis stresses

In the first case the structure is not prestressed at the ambient temperature, while in the second case the structure is prestressed due to the assembly brazing cycle at elevated temperatures. For non-prestressed window structure the stress distribution is shown in Figures 4-13 and 4-14.

The zones of maximum stress are along the braze joint and the lower portion of the cooling channel. The region at the braze joint exhibits high stresses due to the differential in thermal expansion coefficients between the sapphire and the braze and the niobium and the braze. The sapphire and niobium are well matched in their thermal expansion coefficients; however the braze material (a copper-gold alloy) has a higher thermal expansion coefficient than the sapphire and the niobium. The braze therefore experiences compressive stresses along the axis of the braze. The maximum compressive stress of 97.1 MPa occurs at the top of the braze, maximum allowable stress for a braze joint of this kind which is 180 MPa [3, 22]. The secondary high stress zone is along the edge of the cooling channel near the axis of symmetry. The tensile

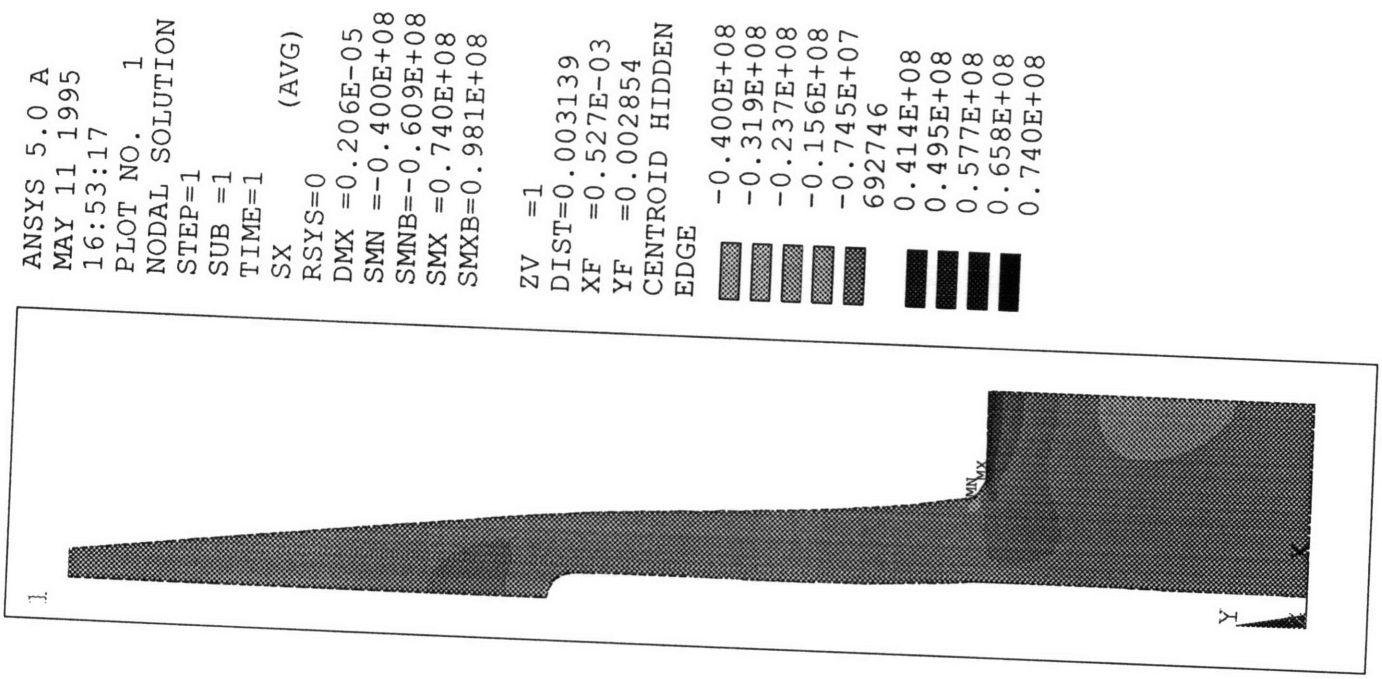

Figure 4-14: Stress Analysis of Distributed Window for 1 MW X-axis stresses

stress at this location is caused by the thermal expansion of the window structure as it heats up and the subsequent deformation, visible in Figure 4-13. The maximum tensile stress in this region is 81.6 MPa, well below the allowable stress for niobium. The General Atomics Distributed Window can therefore securely withstand a 1 MW microwave beam. The only concerns are the manufacture of the window without introducing defects, which the window is susceptible to due to the many braze joints and small scale. The finite element analysis of the window structure illustrates that the distributed window is not limited by thermal runaway and is thermally capable of withstanding a 1 MW microwave beam in the HE_{11} mode in a 10 by 10 cm window structure.

4.4 Diamond Window

The edge cooled diamond window design was investigated using both analytical and finite element analyses. The single disk window design is capable of handling a 1

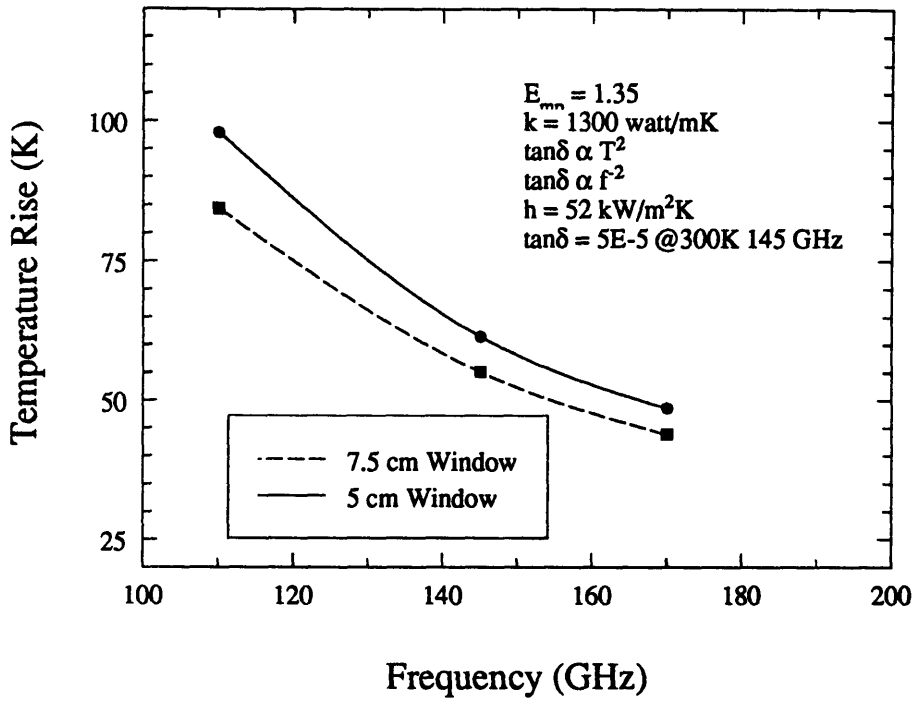

Figure 4-15: Maximum Temperature Rise versus Frequency of the Diamond Window

MW microwave beam in a ring distribution. The maximum temperature rise for a 5 cm window with a ring distribution, a peaking factor of 1.35 and assuming a loss tangent which is proportional to the temperature squared, is 104 K. Although a virtually ideal intensity profile with a very low peaking factor was chosen for the simulation, analytical studies have shown that ring distributions with substantially higher peaking factors would be feasible. A Gaussian beam at the 1 MW level with a peaking factor between 4.1 and 5.6 would cause thermal runaway, due to the high power density and the longer thermal path to the cooling section.

The thermal performance of 5 and 7.5 cm diamond windows was investigated at frequencies of 110, 145 and 170 GHz. The maximum temperature for the two window sizes is shown in Figure 4-15. The decrease in the temperature rise in the 7.5 cm window due to the lower power density and larger cooling surface is quite low and would not warrant a larger diamond disk which would triple the cost relative to the 5 cm window.

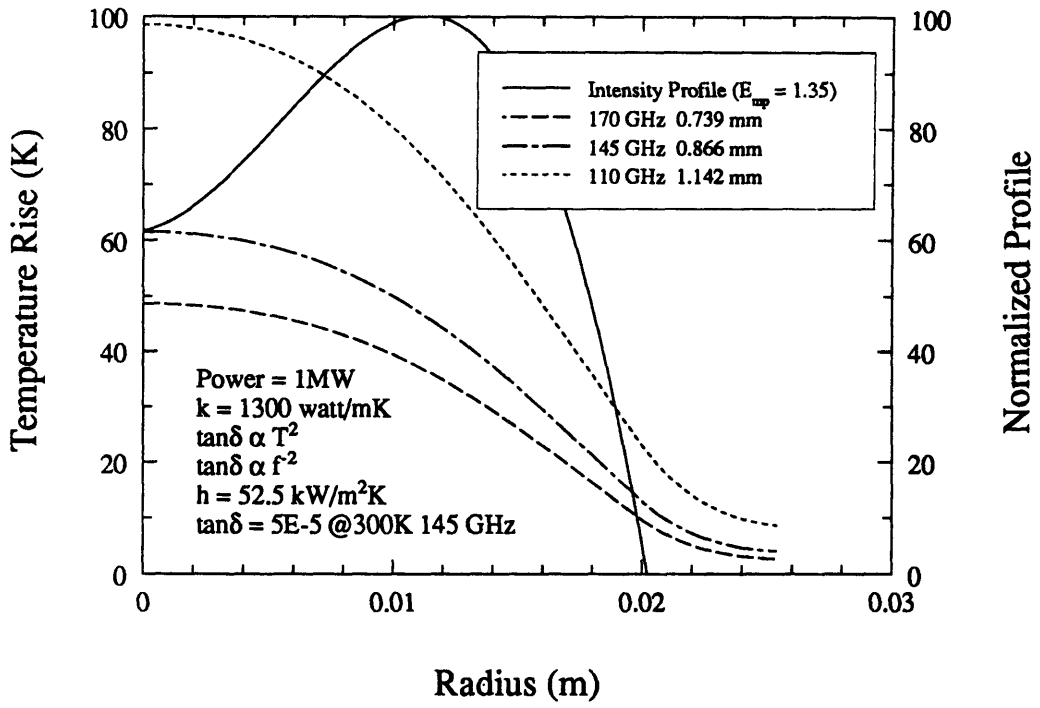

Figure 4-16: Equilibrium Temperature Rise of Single Disk Diamond Window

The temperature versus radius for frequencies of 110, 145 and 170 GHz is shown in Figure 4-16. The temperature distribution for a ring intensity profile assumes a parabolic shape. The maximum temperature rise decreases with frequency due to the loss tangent being inversely proportional to the frequency squared as well as the fact that the window thickness must decrease to remain anti-resonant. The maximum temperature rise for a 170 GHz window at a 1 MW power level would be 48 K at the center.

A 110 GHz 5 cm diamond window structure was also analyzed for its transient response. As shown in Figure 4-17 the 98% rise time is approximately 1 second. The relatively fast transient response is due to the high thermal diffusivity and high heat transfer rate at the cooling channel.

The diamond window design was also examined for mechanical and thermal stresses. The obtained temperature profile was used as input for a stress analysis together with the coolant pressure and the pressure differential across the disk due to the vacuum inside the gyrotron tube. A 110 GHz window with a radius of 5 cm was

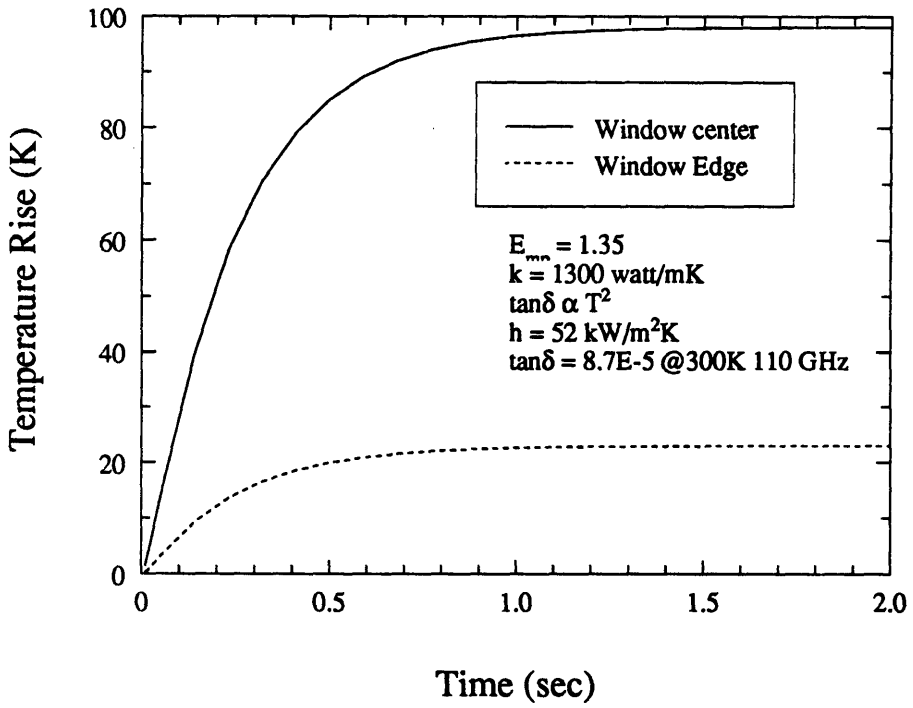

Figure 4-17: Transient Response of 5 cm 110 GHz Diamond Window

considered, to achieve antiresonance a window thickness of 0.1142 cm was chosen. The 110 GHz window experiences the highest thermal loading of the cases considered here due to frequency scaling of the loss tangent. The results of the 2D stress analysis are shown in Figure 4-19 and 4-18. For these stress analyses it was assumed that the window was brazed to a support at the wave guide diameter, the support is also part of the cooling channel. The maximum stresses for this configuration occur at the braze interface between the diamond window and the metal support. The maximum tensile stress is only 35.2 MPa and the maximum compressive stress is 137 MPa. The low magnitude of the stresses is due in part to the low thermal expansion coefficient of the diamond material. The coolant pressure exerted on the window disk is balanced as it is exerted on both faces, this design feature reduces the stress sources to the window temperature rise and vacuum holdoff.

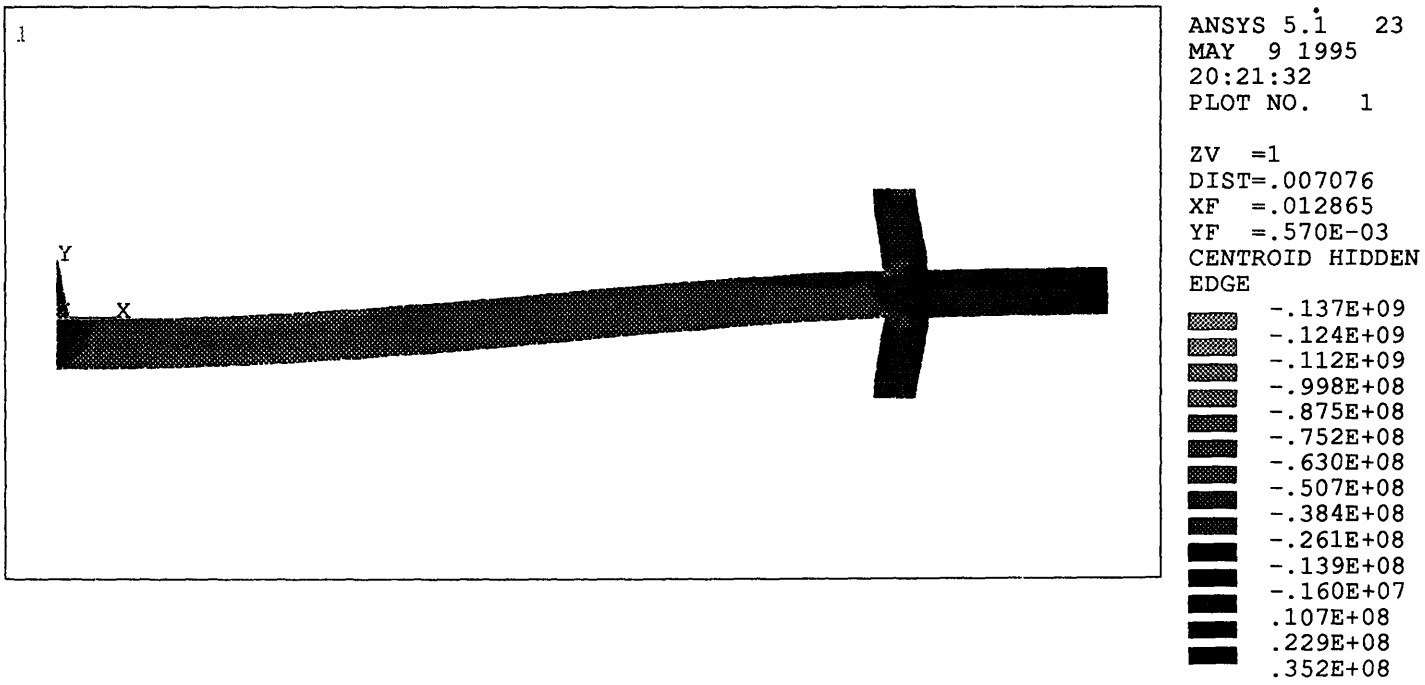

Figure 4-18: Radial Stresses in 5 cm Diamond Window 1 MW (MPa)

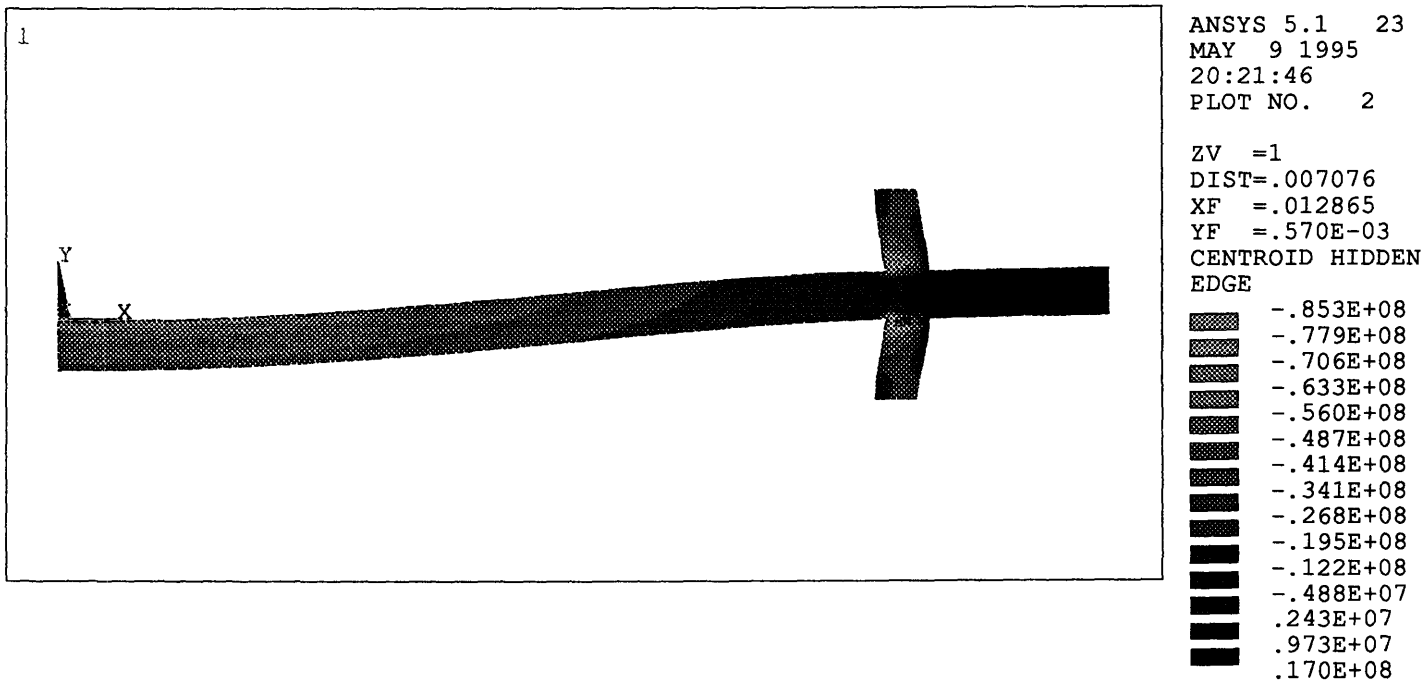

Figure 4-19: Tangential Stresses in 5 cm Diamond Window 1 MW (MPa)

Chapter 5

Conclusion

5.1 Summary of Results

Three different window designs have been analyzed for their thermal and mechanical performances as gyrotron output windows. The experimental temperature measurements have been compared to the theoretical temperature response of the sapphire double disk window. The loss tangent, its temperature dependence and the film coefficient of the double disk sapphire window have been obtained. The experimental values for these parameters, as well as the thermal behaviour of the window are in good agreement with the theoretical data.

The maximum power transmission capability of the double disk window with an improved intensity distribution is approximately 500 kW at 110 GHz. The double disk window is limited by thermal runaway, due to the high temperature dependence of the loss tangent and the limited cooling. An optimization of the window size, cooling conduit and power distribution will provide only marginal improvement in the thermal performance, the 1 MW mark cannot be obtained unless a dual output window is utilized. In such a configuration, the beam would be divided in the mode converter into two 500 kW beams which would travel through separate windows and be recombined further down the transmission line. The double disk window also exhibits the least desirable mechanical performance. The window is operating very close to its mechanical load limit as countless window breakages have illustrated.

For a 1 MW gyrotron a different window design must be utilized. The two candidates are the General Atomics Distributed window and the single disk diamond window, both of which possess a power transmission capacity in excess of 1 MW. The GA window exhibits good thermal behaviour due to the high cooling efficiency. The disadvantage of the window is the high complexity and many braze joints. The small feature size of the window provides a challenge to the manufacturing process, especially when scaling the feature size to a frequency of 170 GHz.

The diamond window design shows promising signs as a 1 MW gyrotron window. It is capable of power levels in excess of 1 MW CW and its thermal performance improves with frequency, due to the frequency dependence of the diamond loss tangent. This makes it an attractive choice for high frequency applications such as ITER. The disadvantages of the window are its high cost and restricted aperture of 4 cm diameter which makes the mode converter design more challenging, however a 6.5 cm aperture could be utilized at a higher cost. The high cost of the window material should be balanced to some extent by the simplicity of the window structure. The window exhibits good mechanical properties due to the high strength of the diamond material. The low thermal expansion coefficient makes thermal stresses a relatively minor issue.

In conclusion, it has been established that there are microwave window designs available capable of handling the thermal and mechanical loading in a 1 MW CW gyrotron.

Bibliography

[1] 3M, St. Paul. *Fluorinert Electronic Liquids*, 1981.

[2] S.C. Bates and L Liou. High performance sapphire windows.

[3] W. Beitz and K.H. Küttner, editors. *Taschenbuch für den Maschinenbau / Dubbel.* Springer-Verlag, Berlin, 1990.

[4] V.B. Braginsky, V.S. Ilchenko, and Kh.S. Bagdassarov. Experimental observation of fundamental microwave absorption in high-quality dielectric crystals. *Physics Letters A*, 120:300–305, 1987.

[5] Crystal Systems, Salem, Ma. *HEM Sapphire.*

[6] W. Dienst, T. Fett, R. Heidinger, H.D. Röhrig, and B. Schulz. Investigations on ceramic materials for fusion technology. *Journal of Nuclear Materials*, 174:102–109, 1990.

[7] M.K. Ferber, H.D. Kimrey, and H.D. Berger. Mechanical reliability of ceramic windows in high frequency microwave heating devices. *Journal of Material Sciences*, 19:3767–3785, 1984.

[8] V. Gnielinski. *Int. Chem. Eng.*, 16:359, 1976.

[9] R. Heidinger. Dielectric properties of sapphire for iter ech window develpoment. *Kernforschungszentrum Karlsruhe*, 1994.

[10] R. Heidinger. Dielectric property measurements on cvd diamond grades for advanced gyrotron windows. *Kernforschungszentrum Karlsruhe*, 1995.

[11] D.J. Hoppe, R.M. Perez, and S.D. Glazer. Temperature measurements of a high-power microwave feedhorn window. *IEEE Transactions on Instrumentation and Measurement*, 39:501–503, 1991.

[12] H. Huey, N. Lopez, and G. Hu amd L. Mundie. Infrared monitoring of gyrotron windows. *Varian Associates, Palo Alto*, 1984.

[13] F.P. Incropera and D.P. DeWitt. *Fundamentals of Heat and Mass Transfer*. John Wiley and Sons, New York, 1986.

[14] A. Kasugai, K. Sakamoto, K. Takahashi, K. Yokokura, M. Tsuneoka, S. Maebara, T. Kariya, Y. Saito, T. Yamamoto, and T. Imai. High power transmission experiment on cyrogenic window and double disk window for ecrf system. US-Japan Workshop on RF heating technology, 1994.

[15] J.A. Kong. *Electromagnetic Wave Theory*. Wiley-Interscience, New York, 1986.

[16] K.E. Kreischer. *High Frequency Gyrotrons and their Application to Tokamak Plasma Heating*. Ph.D Thesis, Cambridge, Ma, 1981.

[17] C. Moeller, 1994. General Atomics, private communication.

[18] L.F Moody. *Trans. ASME*, 66:671, 1944.

[19] H.U Nickel and R. Heidinger. A survey of vacuum-windows for high-energy millimeter-wave systems in fusion experiments. In *Proceedings of the 20th Symposium on Electromagnetic Windows*, pages 62–71, Atlanta, Georgia, 1992.

[20] V.V. Parshin. Dielectric materials for gyrotron output windows. *International Journal of Infrared and Millimeter Waves*, 15:339–348, 1994.

[21] R. Temkin. Comparison of double disk window designs. unpublished results, 1994.

[22] V.V. Teslenko. Bonding of sapphire with metals. *Elektrotekhnika*, 62:63–66, 1991.

[23] Y.S. Touloukian and C.Y. Ho, editors. *Thermophysical Properties of Matter*, volume 2, Thermal Conductivity of nonmetallic Solids. Plenum Press, New York, 1972.

[24] J.-G. Wégrowe, F. Moons amd M. Vassiliadis, and E. Zolti. Limits of operation of conventional rf windows for electron cyclotron wave launchers in a reactor. In *14th Symposium on Fusion Technolog*, pages 821–827, Avignon, France, 1994.